Journal of Earthquake Engineering

ISSN: (Print) (Online) Journal homepage: https://www.tandfonline.com/loi/ueqe20

Low-Damage Rocking Precast Concrete Cladding Panels: Design Approach and Experimental Validation

Jitendra Bhatta, Rajesh P. Dhakal, Timothy J. Sullivan & Mark Lanyon

JOURNAL OF EARTHQUAKE ENGINEERING
https://doi.org/10.1080/13632469.2020.1830201

Low-Damage Rocking Precast Concrete Cladding Panels: Design Approach and Experimental Validation

Jitendra Bhatta [a], Rajesh P. Dhakal [b], Timothy J. Sullivan [b], and Mark Lanyon [c]

[a]Department of Civil Engineering and Natural Resources Engineering, University of Canterbury, Christchurch, New Zealand; [b]Department of Civil and Natural Resources Engineering, University of Canterbury, Christchurch, New Zealand; [c]Lanyon and LeCompte Construction Limited, Christchurch, New Zealand

ABSTRACT
This paper presents the development (concept, design, detailing, and fabrication) and experimental validation of a novel low-damage precast concrete cladding panel system that can accommodate significant inter-story drift demand through the rocking mechanism of the panels facilitated by smartly designed connections between the panels and the structural members. Two adjacent in-plane panels separated by 'one-stage' sealant joint were subjected to in-plane quasi-static cyclic drifts. The cladding system suffered no damage until 1.92% inter-story drift when the sealant tearing occurred. Furthermore, comparison with the seismic performance of traditional panel connections, reported in the literature, also demonstrated the system's significantly improved seismic resilience.

ARTICLE HISTORY
Received 6 May 2020
Accepted 23 September 2020

KEYWORDS
Low-damage system; architectural cladding; precast panels; rocking; cyclic loading

1. Introduction

One of the main objectives of the New Zealand Building Code is to ensure that buildings meet 'life-safety' performance requirements (MBIE 2004). To this extent, modern buildings generally demonstrated good resistance to collapse during the recent earthquakes in New Zealand (NZ) (including the 2010–11 Canterbury, 2013 Seddon, 2014 Castlepoint, and 2016 Kaikoura earthquakes). However, damage to non-structural elements has been persistent during these events (Baird 2014; Baird and Ferner 2017; CERC 2012; Dhakal 2010; Dhakal, MacRae, and Hogg 2011; MBIE 2017). The total estimated cost of rebuilding Christchurch and its surrounding areas after the Canterbury Earthquakes is reported to be approximately 40 billion USD (English 2015; Wood, Noy, and Parker 2016). Bradley et al. (2009) have shown that a considerable portion of the total economic losses due to an earthquake can be attributed to damage to 'non-structural' elements.

'Non-structural' elements are those secondary systems or components attached to the floors, roofs, and walls of a building or industrial facility that are not part of the main vertical or lateral load-resisting structural systems but are required to resist the effects of seismic actions (Villaverde 1997). Suspended ceilings, external cladding and glazing systems, internal partition walls, doors/windows, chimneys, parapets, sprinkler systems, and other building services fall into this category. These non-structural components cost much more than the structural systems for most types of buildings (Khakurel et al. 2020; Taghavi and Miranda 2003). Among the 'non-structural' elements, the cladding or façade system can cost up to 18% of the building's initial cost (Lam and Gad 2002; Taghavi and Miranda 2003).

The architectural precast concrete cladding has been a feature of many NZ buildings since the mid-twentieth century (for example German Embassy and Civic Administration Building in Wellington; Simu and Old Telecom Building in Christchurch) (CCANZ 1992). Unfortunately, most of these

CONTACT Jitendra Bhatta jitendra.bhatta@pg.canterbury.ac.nz Civil Engineering and Natural Resources Engineering, University of Canterbury, Christchurch 8140, New Zealand

This article has been republished with minor change. This change do not impact the academic content of the article.

buildings are either demolished or closed due to the 2010/11 Canterbury and 2016 Kaikoura Earthquakes. Nevertheless, over recent decades, precast concrete cladding panels have been extensively used in modern non-residential buildings throughout NZ (Baird 2014; Curtis 2014; Khakurel et al. 2019; Page 2009).

In seismically active zones, precast concrete cladding systems are characterized by connections (including bearing/gravity connections of the panel, and connections between the panel and the structure to control the movements of the panels) and joints between the adjacent panels. The periphery around the connections and joints are found to be among the frequently damaged regions of precast concrete cladding systems (Folić 1991). Precast panels have been generally either fully-uncoupled ('isolated system') or partially coupled ('dissipative systems') from the movements of flexible structures either through a 'translation' mechanism (Wang 1987; Hutchinson et al. 2014; Baird 2014) or a 'rocking' mechanism (Cohen 1995; Dal Lago 2015; McMullin et al. 2012; Negro and Tornaghi 2017; Wang 1987). These mechanisms tend to avoid stresses, which, otherwise, can lead to fastening failures and damage to expensive and brittle concrete panels. The construction of precast panel systems that accommodate inter-story drifts undergoing rocking mechanism is a common practice in Japan (Cohen 1995; Wang 1987). They have been experimentally proven to perform satisfactorily without any visible damage to panels and their fastenings under seismic actions (Wang 1987). According to Wang (1987), their practice is sparse outside Japan, possibly because of their intricate details, susceptibility to installation errors, and higher costs. Nevertheless, several recently published research on the rocking arrangements of the panels with some energy dissipative connections tested in Europe (Dal Lago 2015; Negro and Tornaghi 2017; Toniolo and Dal Lago 2017) demonstrate the outspread and advancement of rocking precast panels with promising results.

In NZ and the US, it is a common practice to 'isolate' the precast cladding panels from movements of a flexible structure through tie-back (slotted/oversized holes) or push-pull (flexible threaded rod) connections (PCI 2007 ; ASCE/SEI 2010). In NZ, the more prevalent practice is to provide slotted tie-back connections (Massey, Megget, and Charleson 2007), as shown in Fig. 1, near the top of the panels. These connections allow relative movement between the panels and the structure while resisting the out-of-plane seismic loads. Both the gravity loads and out-of-plane seismic forces are resisted by the bearing connections (Fig.1 and Fig. 2) located at the bottom of the panels (generally welded to the structure).

Unfortunately, connections for precast concrete panels were generally found to have insufficient capacity to accommodate the seismic deformations of the primary lateral structural system during earthquakes (MBIE and EQC 2017). The slotted connections were reported to have performed poorly

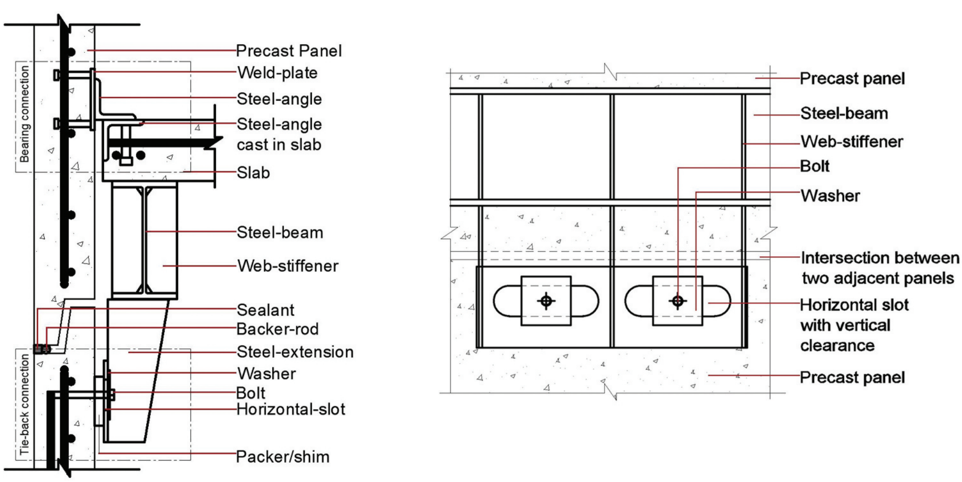

Figure 1. Sliding tie-back connection. a. Side view; b. Rearview

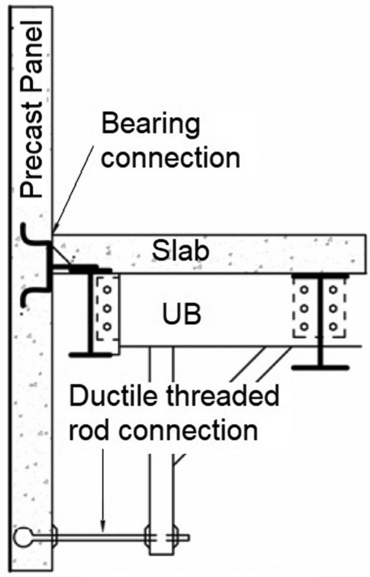

Figure 2. Ductile threaded rod connection (Massey, Megget, and Charleson 2007).

concerning their design intent during the recent Canterbury Earthquakes (SESOC 2019). In some cases, they were either poorly installed or inadequately detailed leading to overstraining of connections during earthquakes. Such overloading of connections can ultimately lead to connection failure (Folić 1991) and, consequently, leave the panels precariously hanging with imminent danger to life-safety and collapse (Baird, Palermo, and Pampanin 2011; Baird 2014; SESOC 2019).

There is also a concern that long-term environmental effects could worsen the performance of such connections. The sliding mechanism can gradually impede due to rusting and corrosion in the slot (Hunt 2010; Wang 1987) or lock due to twisting/bending of the steel components (Baird 2014). Even hot-dipped galvanized steel connections, when in contact with mortar, concrete, or unlike/dissimilar metals (giving rise to bimetallic corrosion), are found to corrode (Maness 1991).

On the other hand, panels with long flexible threaded ductile rods (Fig. 2) accommodate the inter-story drifts through the bending of the rods. They are practical in situations where a more significant gap is needed between the panels and the structure (Massey, Megget, and Charleson 2007). Even though their seismic performance is found to be superior to that of the slotted connections, they are susceptible to low-cycle fatigue (Baird 2014; Massey, Megget, and Charleson 2007; Pantoli 2016; Rihal 1989; Sack, Beers, and Thomas 1989; Wang 1987).

The bearing connections which are usually welded to the structure need adequate tolerances and space for easy and efficient welding. The extreme heat from the welding of steel components, especially stainless-steel, can lead to potential cracking in the nearby panel and concrete frame due to abrupt expansion of concrete, promoting long-term deterioration. Moreover, the finished surfaces of the panels can easily get stained from sparks and smoke during field welding (ACI 533R-93 1993; CCANZ 1992) recommends avoiding fully welded fixings as they require close supervision, cannot accommodate movement, and require a subsequent coating to prevent corrosion. Zinc-rich paints are generally recommended to be applied over welded areas after welding galvanized steel (PCI 2007).

The width of joints and the joint material used between adjacent panels also affects the panels' ability to accommodate the differential movements between the panels. In traditional panel systems utilizing tie-back or push-pull connections, large differential movements are expected at a building corner where the panels on different sides of the building meet. Therefore, a large vertical joint is provided at building corners (Hutchinson et al. 2014) to accommodate such movements. Field-molded sealants with low a b

Figure 3. Precast concrete panel failure in 2010–11 Canterbury Earthquakes (Baird 2014). a. Detached coffered precast concrete panel; b. Collapsed panels

modulus of elasticity (such as polysulfides, polyurethanes, and silicones) are generally interjected in the joints for weather resistance (PCI 2007).

Even though most precast concrete cladding panels performed well from a life-safety point of view during recent earthquakes in NZ, some collapsed panels (Fig. 3) posed a significant threat (Baird 2014; SESOC 2019). It is, therefore, important that the design and detailing of the panel-to-structure connections ensure that their strength and displacement capacity are adequate to meet the corresponding seismic demands, at least, during design level earthquakes. For cladding systems, inter-story drift is typically considered as the engineering demand parameter to characterize their performance levels (FEMA E-74 2011). Several standards, such as NZS 1170.5 – Supp1 (2004), EC8 (2004), and FEMA *P*-750 (2009), suggest inter-story drifts or deformation limits that different cladding systems can accommodate before the onset of damages. However, the definition of such deformation limits is vague and imprecise (Baird 2014).

Therefore, for a seismically resilient and economically attractive solution, there is a need for a precast cladding panel system that offers better control over its overall seismic behavior. Moreover, it should also enable quick and easy installation and adjustments of panels, which ultimately reduce the on-site welding, manual labor, and crane time. A novel low-damage precast concrete cladding system is developed in this research utilizing slotted steel-embeds and weld-plates cast into the panels as rocking connections. These connections can be detailed to ensure the cladding panels remain undamaged until the design drift demand is achieved. The novelty lies in providing the vertical slot within the panels, filling the slot with grease to avoid corrosion over time, reducing on-site welding, three-dimensional tolerances, and overhanging RHS bearing connections. This paper presents the concept, design procedure, fabrication, installation, and experimental validation of the low-damage rocking precast cladding system.

2. Novel Rocking Connections and Their Design Philosophy

2.1. Novel Rocking Connection Details

The new rocking connections details, shown in Fig. 4, are comprised of two main components: two weld-plates and four steel-embeds with vertical slots. Each weld-plate consists of a rectangular Mild-Steel (MS) plate with reinforcement bars welded to it (hence the name) to anchor the plate to the panel. Similarly, each 'steel-embed' consists of an MS plate with a sufficiently long vertical slot (to cater to the inter-story demands), four steel studs, a cap, a bolt, and a washer. The steel studs (plug-welded to the MS plate) primarily resist the out-of-plane loads. The cap (a "U"- section with thin sides) is attached over the slot at the rear face of the MS plate after placing washer and bolt into the slot. The cap can be made either from sheet-metal, channel section, fiber-glass, or any suitable solid material that can serve

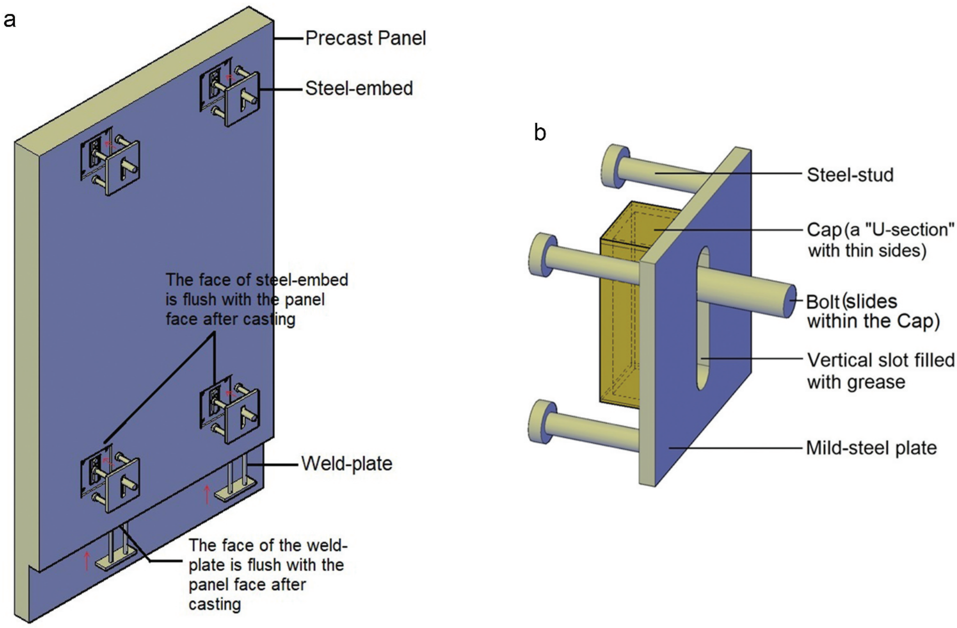

Figure 4. Steel-embed and weld-plate. a. Precast panel with steel-embeds and weld-plates; b. Steel-embed

as a guide for sliding of the bolt. The cap can be welded or epoxied at the back of the MS-plate, encasing the bolt-head and the washer. Grease is injected into the slot to aid the sliding mechanism and prevent overtime rusting of the steel slot. Furthermore, the high evaporating point of grease avoids its frequent replenishing for an extended period.

The steel-embeds and weld-plates are entirely cast into the panel with the face of these plates flushed with the panel's face during the manufacturing process at locations shown in Fig. 5. It is recommended to support the weight of the panel at one level by no more than two connection points to keep the panel cross-section in compression (ACI 533R-93 1993; CCANZ 1992; PCI 2007). Otherwise, the deformation of the supporting frame members may cause the panel weight to be distributed differently than that assumed in the calculation and compromise their performance (PCI 2007). CCANZ (1992) also recommends a minimum of four fixings to transfer lateral loads due to wind and earthquake. Therefore, the four steel embeds are provided to resist the out-of-plane seismic actions, which also oppose the in-plane loads. In this configuration, rectangular hollow sections act as bearing connections (described later), which protrude from the structure to resist the gravity load of the panel. The slotted steel-embeds allow the rocking motion in the panels. The weld-plates in the panel rest on top of the bearing connections and avoid local spalling and chipping of panels during rocking.

2.2. Design of the Vertical Slot in the Steel-embed for Inter-story Drift Capacity

A panel of height 'h' and width 'b' with the proposed 'rocking' connection: steel-embeds with vertical slots 'v_a', 'v_b', 'v_c' and 'v_d' and weld-plates resting on bearing connections protruding from the structure at 'A' and 'B' is considered in Fig. 5. The bearing connections are located at height '$h_{1'}$ from the base of the panels. The top steel-embeds 'v_a' and 'v_b' and the top of the panel are located at height 'h_e' and '$h_{2'}$ above the bearing surface (i.e., at the weld plate), respectively. Note that '$h_{2'}$ is approximately equal to the floor height 'H' for full-story high panels.

The steel-embeds are connected to beams/slabs via bolts. When the top beam displaces laterally by a distance 'ΔH' towards the right relative to the base of the panel, the steel-embeds 'v_a' and 'v_b' are expected to move simultaneously with the top beam in the same direction.Rocking of the panel about

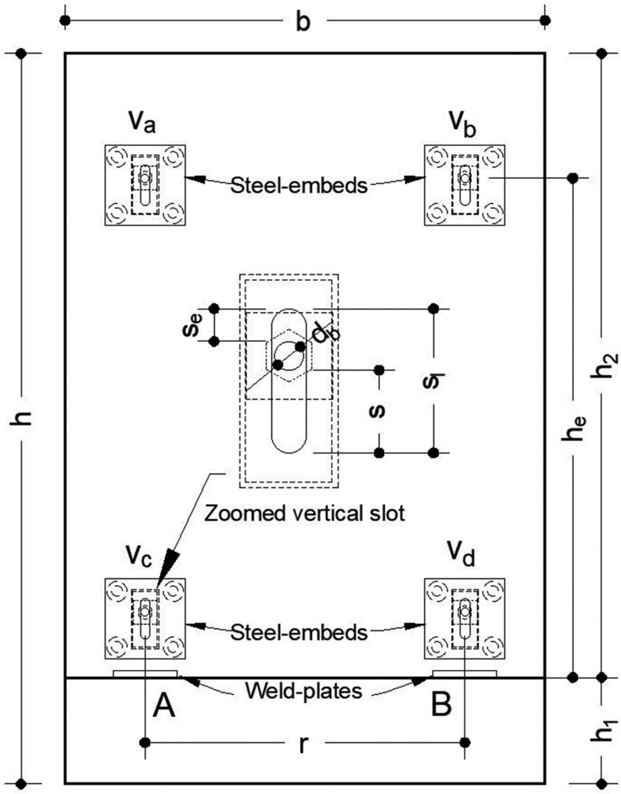

Figure 5. Panel with novel rocking connections (not to scale).

'B', uplifting of the panel edge near 'A' by 'ΔV', causes a downward vertical movement of the bolts in steel-embeds 'v_a' and 'v_c', as shown in Fig. 6. The movement of the bolts in the vertical slots is also shown for clarity in Fig. 6. The bolts in 'v_b' and 'v_d' are expected to undergo slight vertical movement during this rigid body motion since they are close to the vertical line of rotation.

It is to be noted that sufficient frictional force must be developed at the point of rotation for the panels of height '$h_{2'}$ above the bearing points (or point of rotation 'O') and width 'b' to rock. Assuming that lateral force (F) is acting at the top steel embeds at a height 'h_e' of the panel from the point of rotation 'O', as shown in Fig. 7. Taking moment equilibrium about 'O' gives:

$$F \times h_e = W \times b/2 \tag{1}$$

where, 'W' is the weight of the panel.

$$\Rightarrow F = \frac{W}{2(h_e/b)} \tag{2}$$

Considering equilibrium of the horizontal forces,

$$F = \mu W \tag{3}$$

where, 'μ' is the coefficient of friction between the contacting surfaces at the bearing points. From Equations 2 and 3,

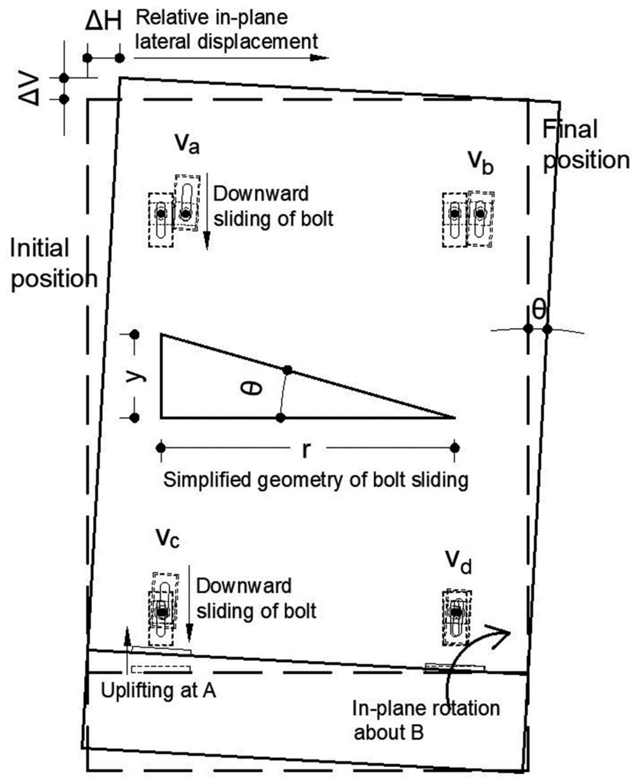

Figure 6. In-plane rotation of panel.

$$\mu W = \frac{W}{2(h_e/b)} \Rightarrow \mu = \frac{1}{2(h_e/b)} \tag{4}$$

Therefore, the minimum friction coefficient required for a panel to start rocking is:

$$\mu_{min} = \frac{1}{2((h_2/\alpha_e)/b)} = \frac{\alpha_e}{2(h_2/b)} \tag{5}$$

where, $\alpha_e = h_2/h_e$. 'α_e' can vary depending upon the height and location of the top steel-embeds in the panels.

If the friction coefficient is insufficient, then the panel will slide before the rocking starts. However, ideally, any sliding that occurs can only continue until the bolt touches the edge of the slots in 'v_c' or/and 'v_d'. After that, the bolts in the steel-embeds 'v_c' and 'v_d' resist the additional lateral forces acting as shear keys at the bottom of the panels and then trigger the rocking motion of the panels.

A concern one might have is that controlling the connection strength would be easier than the friction. For example, explicitly designing the steel embeds 'v_c' and 'v_d' to allow initial sliding and then to act as shear keys to initiate the rocking motion of the panel may be an alternative. However, if a horizontal allowance of 'a' (in either direction) is provided in the bottom steel-embeds 'v_c' and 'v_d'. then the inter-story drift that can be accommodated (in a panel of height 'h' under the initial sliding) before the friction between the bolt and edges of the slot starts opposing the rocking motion of the panels, is 'a/h'. On the contrary, if rocking is allowed rather than immediate sliding, the inter-story drift accommodated is 'a/t', where 't' is the height of the bolt from the bearing points in the steel-embeds 'v_c' and 'v_d'. Consequently, by initiating the rocking of the panels by controlling the friction, substantially larger drift capacity could be provided, by a factor of 'h/t'.

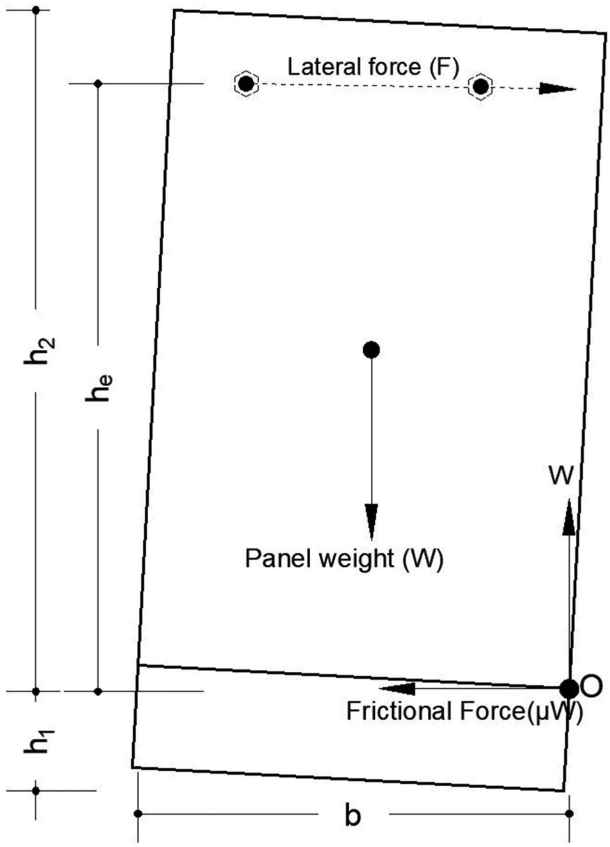

Figure 7. Forces acting on the panel at a rotated position.

Questions about the value of friction coefficient may also be raised and different values of the friction coefficients between several materials in-contact have been provided in Barrett (1990). If the required friction coefficient is considered impractical, a serrated weld-plate could be prepared, and another serrated plate welded on the top of the RHS bearing. In this way, the bearing mechanism (i.e., serrations acting as shear keys) would initiate the rocking, and the dependence on friction is then overcome.

Next, the length of the vertical slot 's_l' in the steel-embeds required to primarily accommodate in-plane inter-story design drift, out-of-plane inter-story design drift, and construction and installation errors can be determined as follows.

If the bolt slides by 'y' at an in-plane inter-story drift of 'θ' as shown in the simplified kinematics of the bolt sliding in Fig. 6, then,

$$y \approx \theta \times r \tag{6}$$

$$s \approx \theta_d \times r \tag{7}$$

where, 's' is the required clearance below the initial position of the bolt in the vertical slot to accommodate in-plane design inter-story drift ratio 'θ_d'.

Again, if the bolt slides by 'y_o' at a relative out-of-plane drift 'θ_{out}' between the panel and the structural frame, as shown in Fig. 8, then,

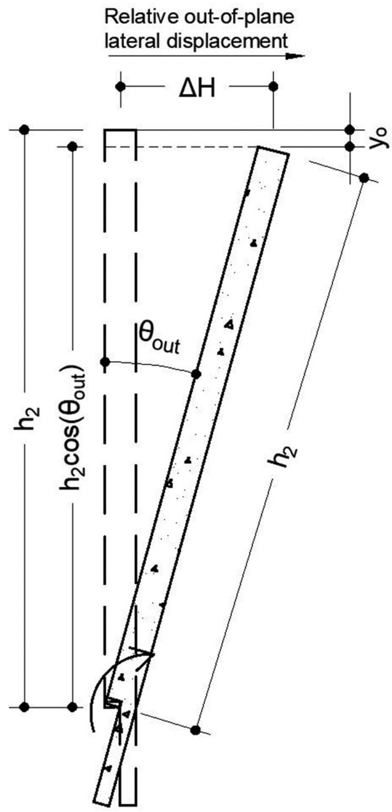

Figure 8. Out-of-plane rotation of panel.

$$y_o = h_2 - h_2\cos(\theta_{out}) = h_2[1 - \cos(\theta_{out})] \tag{8}$$

Then, conservatively in the worst combination of in-plane and out-of-plane deformation,'θ_{out}' can be taken equal to the design drift 'θ_d':

$$\Rightarrow\ s_o \approx h_2[1 - \cos\theta_d] \tag{9}$$

where, 's_o' is the required clearance above the initial position of the bolt in the vertical slot to accommodate the out-of-plane design inter-story drift ratio 'θ_d'.

Furthermore, a vertical tolerance, denoted here as 'e', is required to provide additional construction and installation tolerances and accommodate thermal movements in the structure, connections, and panels.

Finally, the total required length of the vertical slot 's_l' can be obtained for the inter-story design drift 'θ_d' as shown in the zoomed vertical slot in Fig. 5.

$$s_l = s + s_o + e + d_b = s + s_e + d_b \tag{10}$$

where,

$$s_e = s_o + e$$
$$d_b = \text{diameter of the bolt}$$

2.3. Steel-embeds and Weld-plates for the Horizontal and Vertical Design Actions

The procedure adopted in this research for the design of the steel-embeds and weld-plates is described in this section. The design of the steel-embed is based on verifying that each of the steel components and connections can withstand the horizontal design seismic actions prescribed in NZS 1170.5 (2004). The steel embeds are designed following the methodology provided in Hutchinson et al. (2014) and several standards: NZS 3404 (1997), ASCE/SEI (2010), AISC 341-10 (2010), and ACI 318-11 (2011).

- The steel studs are checked for the concrete breakout and their tension capacity considering the out-of-plane design seismic force.
- The Mild-Steel (MS) plate is checked for its weak axis bending capacity, considering the out-of-plane design seismic force.
- The plug-weld between the MS-plate and the steel studs is checked for its shear capacity considering the out-of-plane design seismic force.
- The bolt is checked for its tension considering the out-of-plane design seismic load and shear capacity considering the in-plane design seismic force.
- The washer is checked for its weak axis bending capacity, considering the out-of-plane design seismic force.
- A suitable factor of safety should be imposed on the design of these components.
- The weld-plate is required to withstand the dynamic impact (considering the dynamic impact factors) between the panel base and the bearing connections under seismic vibrations without incurring local cracking/chipping of the panel. The size of the weld-plate to withstand the stress induced by the panels while rocking under a seismic event is calculated based on the vertical earthquake design action as per NZS 1170.5 (Standards New Zealand) (2004). Reinforcing bars are welded to the steel plate to attach it firmly to the panel.

2.4. Width of the Vertical Joint between Panels

When two adjacent story-high panels (labeled as Panel 1 and Panel 2 in Fig. 9) simultaneously rock under relative lateral floor displacements, shear deformation and shear forces are imposed on the sealant at the interface of these two panels as shown in Fig. 9. If the shear deformation in a sealant of width ‘w’ is ‘y’, then the shear-strain in the sealant is given by,

$$\gamma = \frac{y}{w} \tag{11}$$

where, ‘γ’ is the shear strain in the sealant.

When rocking of the two adjacent panels about their bottom-right corners takes place under the applied loads, as shown in Fig. 9, the shear deformation in the sealant ‘y’ can be taken approximately equal to the vertical uplift of the edge of Panel 2 at the interface of the sealant under the inter-story drift of ‘θ_s’. For a critical case, the width of Panel 2 (b_2) is assumed to be longer than the width of Panel 1 (b_1). Assuming rigid panel behavior,

$$\theta_s = \frac{y}{b} \tag{12}$$

where, ‘b’ is taken as the maximum of ‘$b_{1'}$ and ‘$b_{2'}$.

From Equations 11 and 12,

$$\gamma w = b\theta_s \Rightarrow w = \frac{b\theta_s}{\gamma} \; (13)$$

Thus, for a proprietary sealant with ultimate shear strain capacity ‘γ_{ult}’ and story-high panels of width ‘b’, the minimum vertical joint width required to avoid tearing of sealant at an inter-story drift of ‘θ_s’ is:

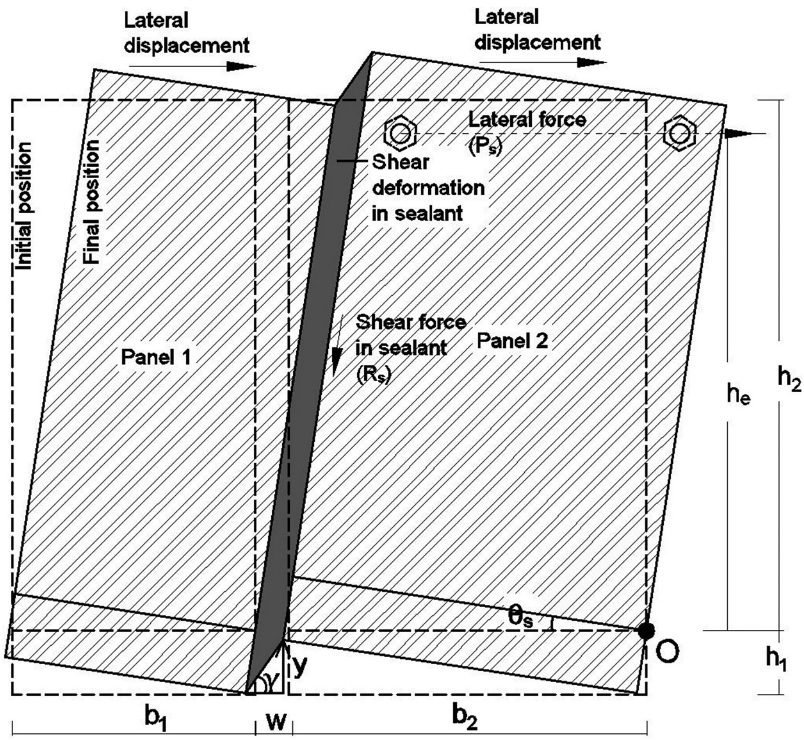

Figure 9. Schematic diagram of rocking panels about their edges and shear deformation in sealant under lateral displacements applied at the top of the panels.

$$w_{min} = \frac{b\theta_s}{\gamma_{ult}} \tag{14}$$

Note that the joint width 'w' is also dependent upon the feasibility of the construction and application of sealant. Dal Lago et al. (2017) identified basic features of silicone under imposed shear strains. Silicone was found to show elastic behavior at shear strains up to a range of 100% to 150% with an average elastic shear modulus of 0.25 MPa. The ultimate shear strain capacity 'γ_{ult}' for a sealant can be obtained from experiments under a controlled environment. However, the properties of the sealant are found to vary with ambient temperatures and the aging of the sealant. Thus, it can be beneficial to consider the time and temperature-dependent properties of the proprietary sealant, if available, for selecting 'γ_{ult}'.

If 'w_f' is selected as the vertical joint gap between the adjacent panels, then 'θ_s' must be corrected to 'θ_{sc}' given by:

$$\theta_{sc} = \frac{\gamma_{ult} w_f}{b} \times 100\% \tag{15}$$

Again, considering that the lateral force at the top steel-embeds of the Panel 2 'P_s' generates a shear force 'R_s' in the sealant during the rocking motion as shown in Fig. 9, then taking moment equilibrium at the bottom-right corner 'O' of the Panel 2 gives,

$$P_s(h_2/\alpha_e) - R_s b_2 = 0 \tag{16}$$

$$\Rightarrow P_s = \frac{R_s b_2 \alpha_e}{h_2} \tag{17}$$

If the height and depth of the sealant are 'h_s' and 'd_s', respectively, then, the shear stress in the sealant 'τ' can be calculated as,

$$\tau = \frac{R_s}{h_s d_s} \tag{18}$$

$$\Rightarrow \tau = \frac{P_s h_2}{b_2 h_s d_s \alpha_e} \tag{19}$$

If '$P_{sealant}$' is the load when the tearing in the sealant takes place, then the ultimate shear stress 'τ_s' can be obtained as,

$$\Rightarrow \tau_s = \frac{P_{sealant} h_2}{b_2 h_s d_s \alpha_e} \tag{20}$$

The shear modulus (G_s) of the sealant is,

$$G_s = \frac{\tau_s}{\gamma_{ult}} = \frac{P_{sealant} h_2}{b_2 h_s d_s \alpha_e \gamma_{ult}} \tag{21}$$

$$\Rightarrow P_{sealant} = \frac{\alpha_e G_s \gamma_{ult} b_2 h_s d_s}{h_2} \tag{22}$$

where, 'γ_{ult}' is the ultimate shear strain capacity of the sealant.

Finally, combining the above-described critical characteristics of the proposed precast concrete cladding panel system with novel rocking connections, its necessary design procedure is summarized in the flowchart shown in Fig. 10.

3. Test Specimen Design and Details

For experimental validation of the design procedure and seismic performance of the developed novel 'low-damage' rocking cladding system, a test specimen comprising two panels (FP1 and FP2) is designed following the above-explained design principles. The panel dimensions and their section details are shown in Fig. 11 and Fig. 12, respectively. The details of the steel-embeds and weld-plates are shown in Fig. 13 and Fig. 14, respectively.

From Equation 10, the clearance below the bolt in the vertical slot is,

$$s = s_l - s_e - d_b$$

In this test specimen, $s_l = 95\,mm$, $s_o + e = 10\,mm$, $d_b = 20$ mm, $h_2 = 1760$ mm

$$\Rightarrow s = 95 - 10 - 20 = 65\,mm$$

Again, from Equation 7,

$$\theta_d = \frac{s}{r} = \frac{65}{r} \times 100\% \tag{23}$$

From Fig. 11,

$r_{FP1} = 1015 - 193 - 193 + 150 = 779\ mm$, $r_{FP2} = 1015 - 208 - 193 + 150 = 764\ mm$

$$\Rightarrow \theta_{d(FP1)} = \frac{65}{779} \times 100\% = 8.34\%$$

$$\Rightarrow \theta_{d(FP2)} = \frac{65}{764} \times 100\% = 8.50\%$$

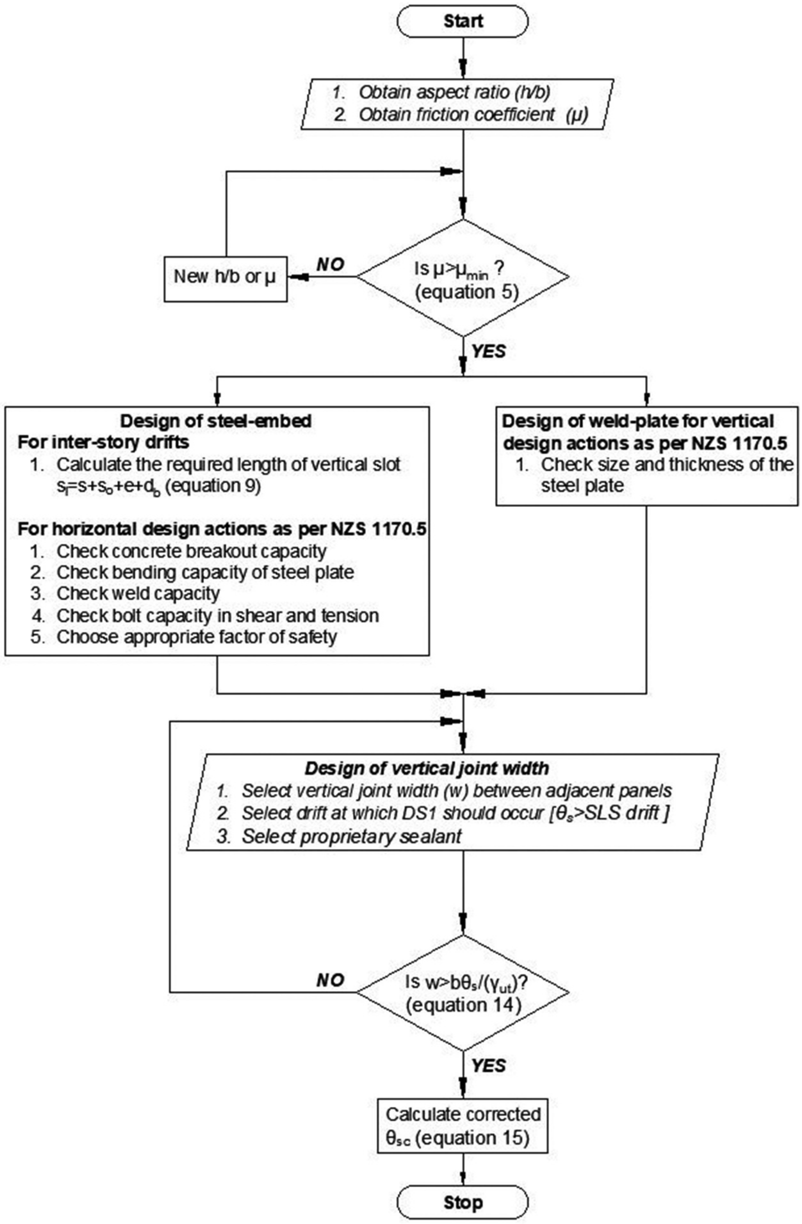

Figure 10. Flowchart showing basic design procedure of panels with rocking connections.

Therefore, it is expected that the slotted steel embeds allow the panels to rock until an inter-story drift of more than 8% without transferring significant forces within the panels.

One may consider this was an overdesign of the drift capacity, as such a drift is not expected in design-level earthquake shaking. However, as this was the first test conducted as a proof of concept on these rocking connections, it was considered prudent to go for an extended slot rather than only for the ultimate limit state of 2.5% inter-story drift (in NZ) to understand its mechanics. It is also evident that as drifts become very large, the panel could begin to strike adjacent architectural features (located on the floor above or at the same floor) if those features are designed to remain stationary when the

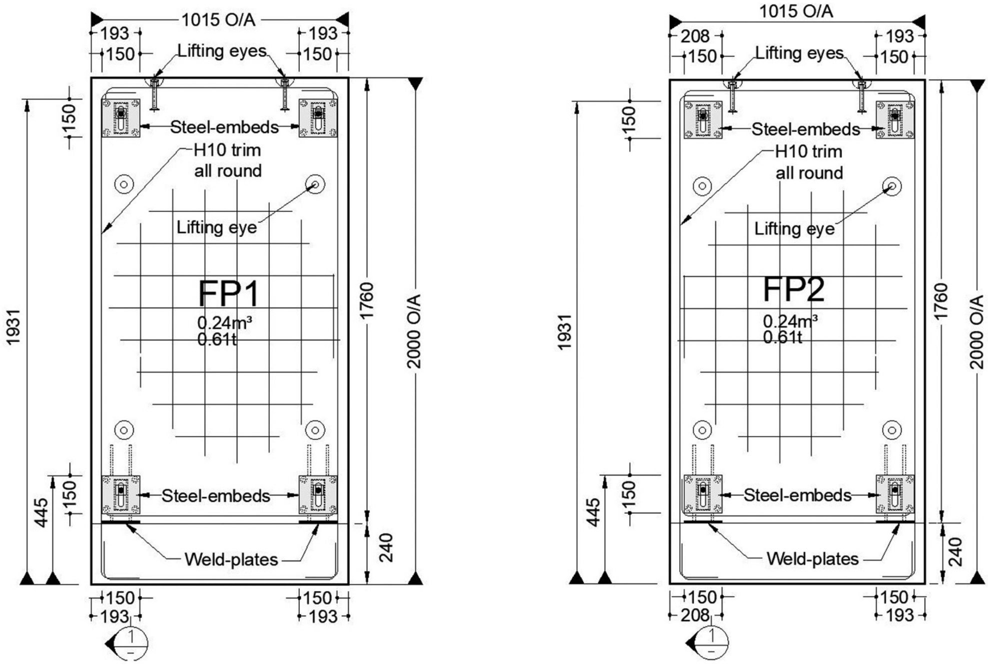

Figure 11. Panel details. a. Panel FP1; b. Panel FP2

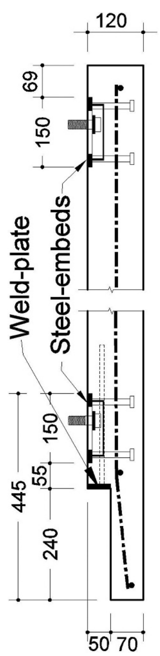

Figure 12. Section-1 (vertical side view) details.

structure sways under the seismic loads. However, this could be prevented if the architectural features are designed to rock, having similar geometrical properties in terms of height, width, and location of their rocking connections.

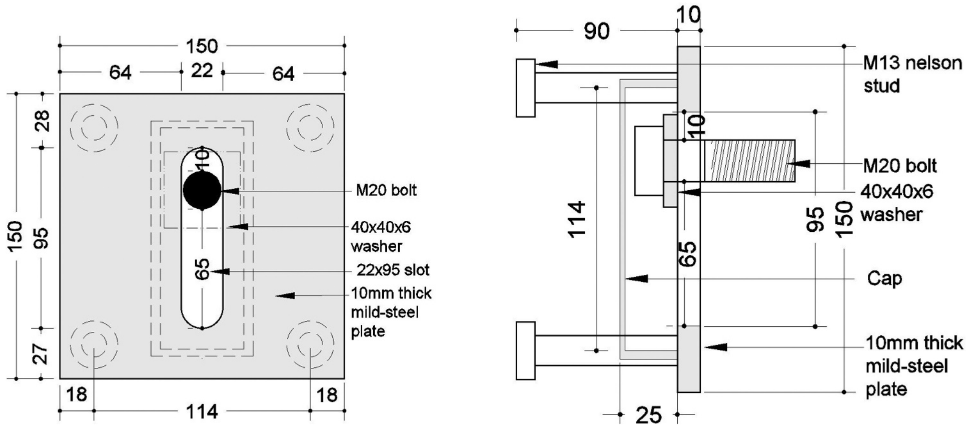

Figure 13. Steel-embed details. a. Front view; b. Side view

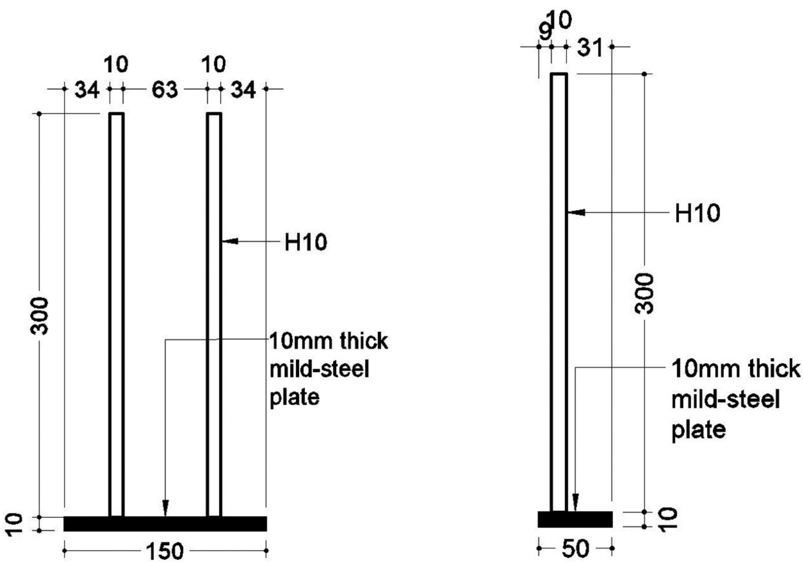

Figure 14. Weld-plate details. a. Front view; b. Side view

The required minimum coefficient of friction between the bearing surface and weld plate can be calculated from Equation 5. From Fig. 11 $h_2 = 1760\ mm$, $h_e = 1671\ mm$ and $b = 1015\ mm$. Therefore, $\alpha_e = h_2/h_e = 1760/1671 = 1.05$

$$\Rightarrow \mu_{\min} = 1.05 \times \frac{1}{2(1760/1015)} = 0.303 \tag{24}$$

Since the weld-plate and bearing connection are of mild steel, the coefficient of static friction between the two surfaces can be taken as 0.74 (Barrett 1990), which is significantly higher than 0.303.

The width of the vertical joint between the panels FP1 and FP2 is determined from Equation 14. Here, the maximum width of the panels is b = 1015 mm. If one assumes, $\gamma_{\mathrm{ult}} = 125\%$ and $\theta_s = 1.50\%$,

$$\mathrm{w}_{\min} = \frac{1015 \times 1.5\%}{125\%} = 12.2\mathrm{mm} \rightarrow 15\mathrm{mm} \tag{25}$$

A vertical joint gap of 15 mm is selected for the test. Hence, the corrected inter-story drift 'θ_{sc}' at which the sealant tearing starts is estimated using Equation 15 as:

$$\theta_{sc} = \frac{\gamma_{ult} w}{b} = \frac{125\% \times 15}{1015} = 1.84\% \tag{26}$$

4. Fabrication and Installation of the Panel Specimens

After the design and detailing of the specimens, the two panels, FP1 and FP2, and their connections were shop fabricated. It is of paramount importance to control the quality of fabrication to assure that the vertical slots are parallel to each other and free of any debris for the satisfactory rocking of the panels, even though the overall geometrical dimensions of panels are challenging to be precise (PCI 2007). Therefore, this requirement is bound to increase the initial construction time and cost. However, builders and practitioners were consulted and they pointed out that the system could anyway be economical compared to the current systems used, as it allows for a quick and easy three-dimensional adjustment and installation of panels, significantly reducing the on-site crane and labor cost and time.

In order to correctly align the fabricated steel-embeds, they were tack welded to steel angle-lines (Fig. 15) at locations provided in the shop drawings of the panels. The angle-lines covered most of the vertical slot, which prevented wet concrete squeezing into the slot. Silicone (Fig. 16) and rags were also used for the same purpose. The threads of the bolts were covered with duct-tape (Fig. 17) to avoid being clogged up with concrete.

The angle-lines with the steel-embeds were then fastened to the formwork at required locations. The weld-plates were also clamped into position (Fig. 18) before pouring the concrete. In addition to

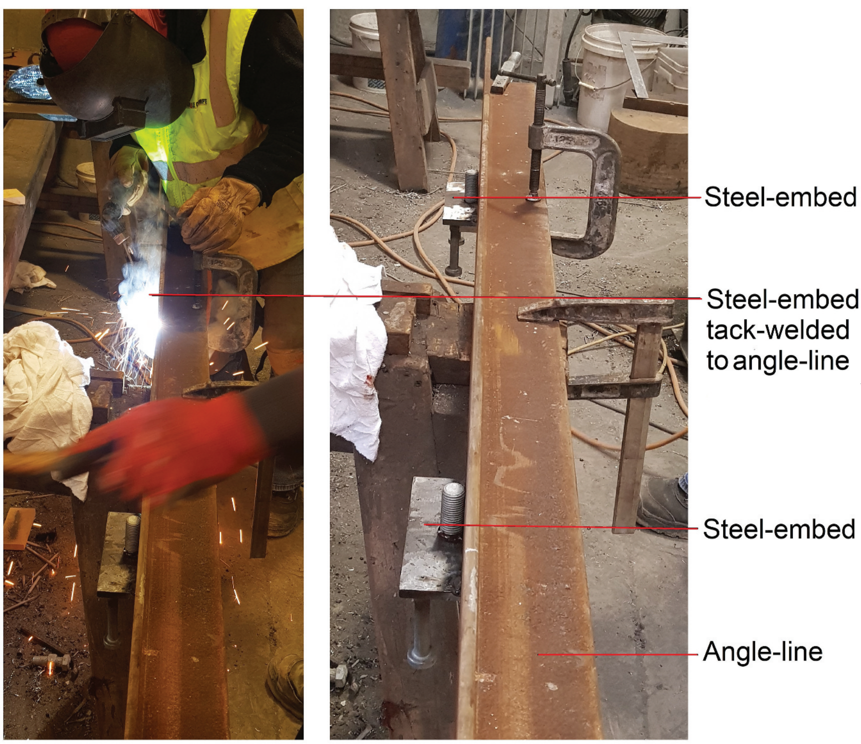

Figure 15. Steel-embeds tack-welded to steel angle-lines.

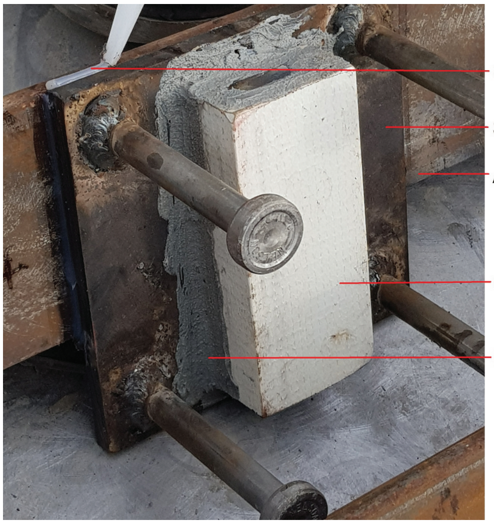

Figure 16. Silicone to seal any openings between angle-line and steel-embed.

Figure 17. Duct-tape to avoid wet concrete clogging the bolt-threads.

these connections, four-anchors for face lifting and two-anchors for top-lifting were placed in the panel. After the concrete cured and achieved the required compressive strength of around 25 MPa, the next day, the steel-embeds were ground off, and the angle-lines were removed. Removal of the angle-lines left cavities (or dents) in the panels, as shown in Fig. 19, which were grouted (Fig. 20) for a smooth finish.

After the panels reached their required compressive strength of 40 MPa, the panels were transported to the structural laboratory at the University of Canterbury. The panels were lifted through top lifting anchors and placed on one of the frames of a 3D-steel test frame, as shown in Fig. 21 and Fig. 22.

The main components of the frame associated with the panel attachment were the horizontally slotted plate (Fig. 23) and the rectangular hollow sections (RHS) for bearing connections (Fig. 24). The horizontal slots provide tolerance in the in-plane direction for panel adjustment during installation.

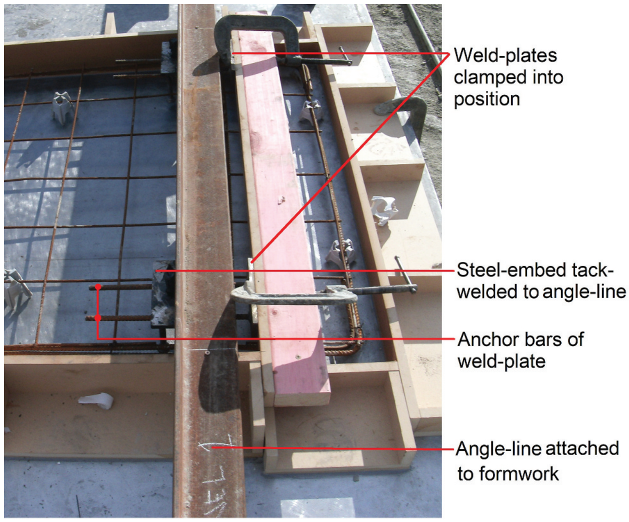

Figure 18. Steel embed and weld-plate placed in formwork.

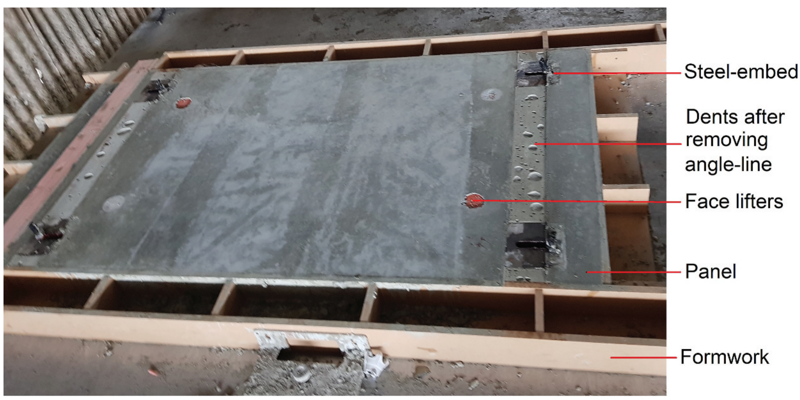

Figure 19. Dents in panel after removal of angle-lines.

The panels were adjusted and aligned using plastic shims (for maintaining the width of the vertical joint in-between the adjacent panels and the gap between the panels and the structure). After the panel FP1 was placed at its position, plastic shims of a total thickness of 15 mm were packed in-between the adjacent panels. At this stage, panel FP2 was still hanging with the help of a crane. However, the bolts in the steel-embeds of panel FP2 were already inserted through the horizontal slot of the slotted-plate connected to the structure. The nuts were slightly tightened to avoid any accidental out-of-plane rotation of the panel. The hanging panel FP2 was then carefully maneuvered using a crane and manual labor. Once the panel acquired the desired configuration/alignment, the bolts were tightened up fully and then were loosened half-a-turn before testing to allow relative movement (primarily in the vertical direction) between the panels and the structure. The plastic shims were then removed, and the washers were tack-welded to fix the panels into position, thereby prohibiting relative horizontal movement between the panels and the structure (therefore, termed as 'horizontally-restrained' bolts).

The weld-plates rested on the RHS bearing connections (welded to the web of the beam). The face of the RHS bearing connections was made slanted to allow out-of-plane rotation of the panels.

The edges of the panels were chamfered to ease sealant application. The joint was filled with a one-stage silicone sealant to a depth of approximately 10 mm (the width-to-depth ratio of 1.5:1).

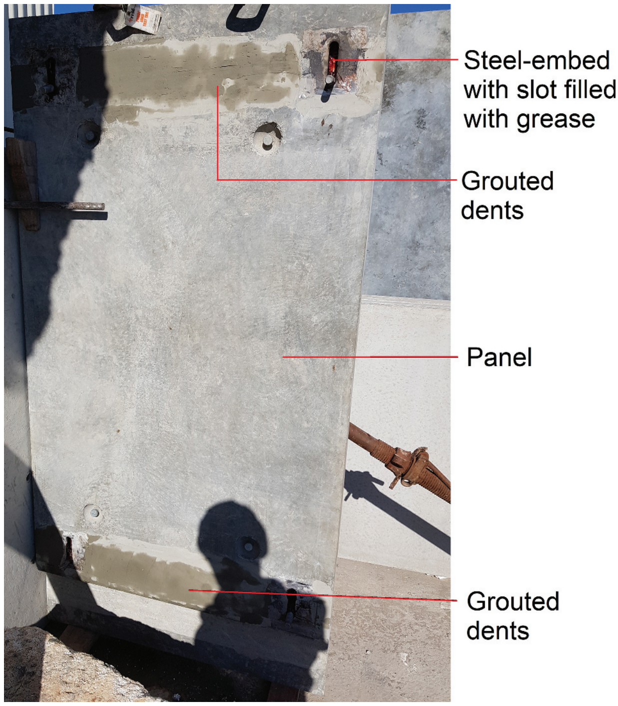

Figure 20. Grouted dents.

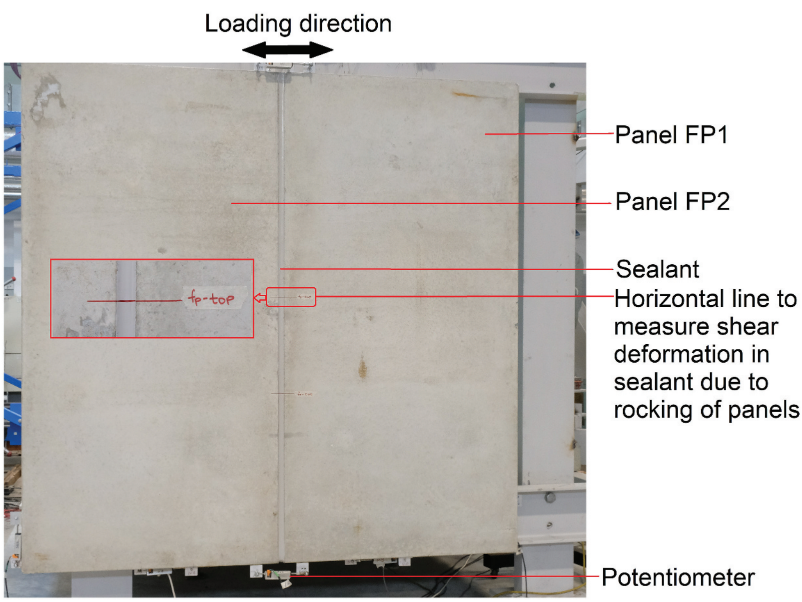

Figure 21. Experimental setup showing front view of panels.

The sealant was left for 19 days to cure fully. PCI (2007) recommends seven days for curing silicone sealant.

The adjustment and installation of the panels were found to be quick and easy, which could potentially reduce the on-site labor and crane time (and cost). The thickness of steel-shims under the

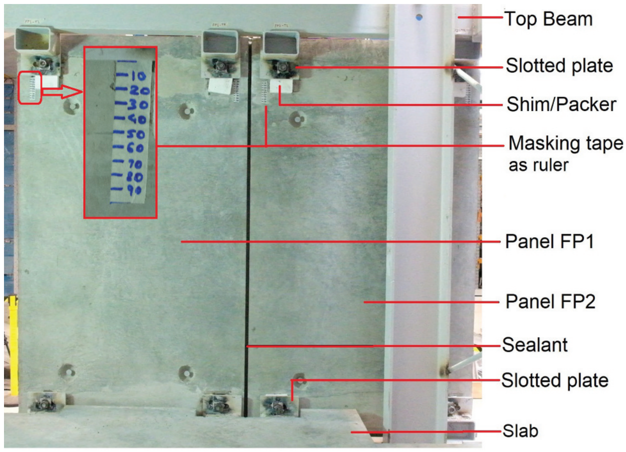

Figure 22. Rearview of the adjacent panels.

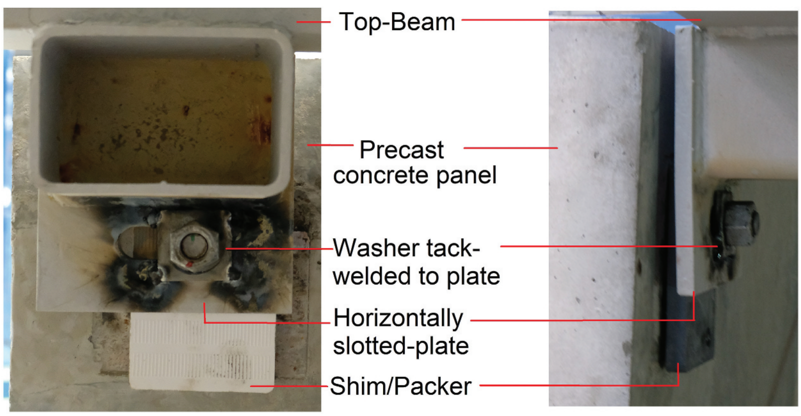

Figure 23. Horizontally slotted plate with 'horizontally-restrained' bolt by tack-welding the washers to the plate.

weld-plates was easily determined by alternately lifting the panel and placing the shims of different thickness underneath the weld-plates (i.e. by trial and error). However, tack-welding the shims on top of the RHS sections was noted to be time-consuming. Therefore, as an alternative, slots could be provided in the panel through slots under the weld-plates, as shown in Fig. 25, to place either plastic or steel shims of standard sizes. The shims could be designed to move with the panel to accommodate panel uplift and then compress down when seated. Some hooks/clips could also be placed over the slot to stop the shims from dislodging in the out-of-plane direction during earthquake shaking. In this way, the labor costs and time associated with welding and crane operations can be avoided.

5. Experimental Setup and Behavior of the Panel System with Rocking Connections

5.1. Instrumentation

A 300kN actuator with a stroke length of ±200 mm was attached to the center of the top slab in order to apply quasi-static cyclic loading. A total of three string-pots were used to record the top-floor displacements. The string-pot located near the top of the frame (attached to the panels) was considered for interpreting the results. The assembly was instrumented with potentiometers to measure the uplift of the panel edges and change in the width of the vertical joint, as shown earlier in Fig. 21. Two

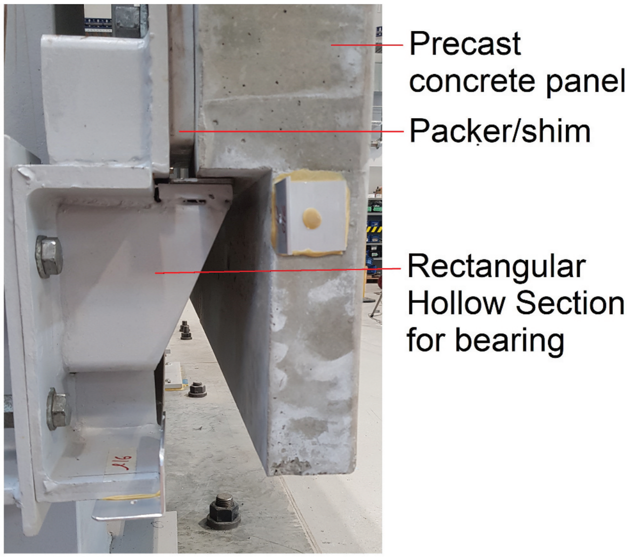

Figure 24. RHS sections as bearing connection.

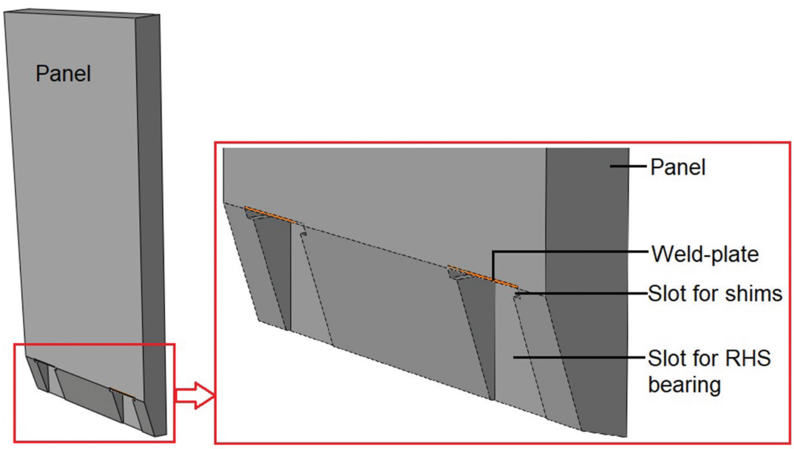

Figure 25. Slot in the panel underneath weld-plate for placement of standard size shims.

horizontal lines were drawn across the vertical joint sealant to measure the shear displacements across the sealant at peak inter-story drifts in each cycle (Fig. 21). Paper masking tape with measurements outlined up to 100 mm, to scale, were adhered near the vertical slot to manually measure the sliding of the bolt in the slot (Fig. 22).

5.2. Characteristic Curve

Under small lateral displacement at the top connections, firstly, the gap present between the bolt and the washer and between the bolt and the edge of the vertical slot in the panel should close. This small displacement can be calculated as:

$$d_{gap} = \left[\frac{(\text{diameter of hole in washer} - \text{bolt diameter})}{2} + \frac{(\text{width of vertical slot} - \text{bolt diameter})}{2}\right] \quad (27)$$

$$\Rightarrow d_{gap} = \left[\frac{22-20}{2} + \frac{22-20}{2}\right] = 2 \text{ mm}$$

Small lateral forces acting at the top connections of a panel are equilibrated by its weight (assuming a sufficient frictional force is developed at the point of rotation) until the forces reach '$\alpha_e Wb/2h_2$'. Where 'W' is the weight of the panel, b' and '$h_{2'}$ are the width and height of the panel above the weld-plates, respectively, as shown in Fig. 5. During this phase, the panel is expected to behave as though it is integrated with the structure, generating high stiffness. When this limit is overcome, the panel starts acting as an 'independent' system to the structure, and it rocks with a constant horizontal force of '$\alpha_e Wb/2h_2$' at the top connections. Under the lateral cyclic displacements, the two bottom edges of the panel rise alternately. In any rotated position, a constant stabilizing horizontal force is provided by the bearing connection on which the panel is seated.

Neglecting the stiffness provided by the interposed sealant between the panels, the required lateral force at the top connections to initiate the rocking of the two panels can be calculated as:

$$P_{panel} = F_o = \sum \frac{\alpha_{ei} W_i b_i}{2h_{2i}} = 2 \times 1.05 \times \frac{6.1 \times 1015}{2 \times 1760} = 3.68\text{KN} \quad (28)$$

where, $W_{FP1}=W_{FP2}=6.1\text{KN}$, $b_{FP1}=b_{FP2}=1015$ mm, $h_{2FP1}=h_{2FP2}=1760$ mm
and

$$\alpha_{eFP1}=\alpha_{eFP2}=h_e/h_2= 1760/1671 = 1.05$$

Finally, after the vertical slots are exhausted at a top lateral displacement 'd_d' corresponding to the design inter-story drift 'θ_d', the stiffness will increase rapidly, resulting in diagonal compression forces in the panels. The post-locking performance of the panels has not been investigated, given that it occurs at a very high inter-story drift of about 8%, in this test, which is very unlikely to happen in actual earthquakes.

The above-calculated displacements and forces serve as characteristic points for the backbone curve for the rocking panels, as shown in Fig. 26.

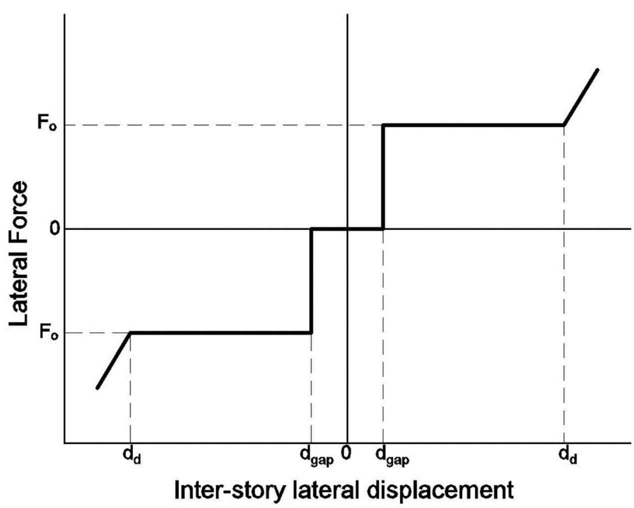

Figure 26. The characteristic curve for rocking panels.

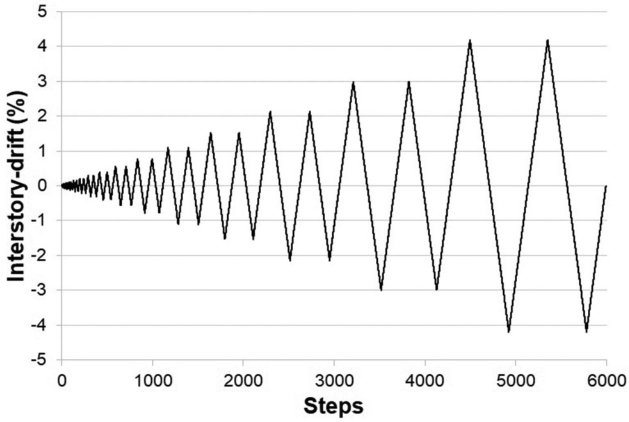

Figure 27. FEMA-461 Loading Protocol (FEMA 2007).

5.3. Experimental Results and Discussion

The pair of adjacent panels, FP1 and FP2, were subjected to increasing levels of lateral cyclic drift, following FEMA 461 (FEMA 2007) loading protocol up to 4.18% inter-story drift, as shown in Fig. 27.

The inter-story drifts and their corresponding lateral forces are shown in Fig. 28. The loading first starts (in the negative direction) with some initial stiffness as panels are engaged. The rocking response of panels at the peak of the final inter-story drift cycle is shown in Fig. 29. The two panels rocked simultaneously, tearing the sealant in shear, but the change in the width of the joint was found to be negligible as the bolts of the top and bottom connections were restrained from moving horizontally by tack-welding the washers (termed as 'horizontally-restrained' bolts).

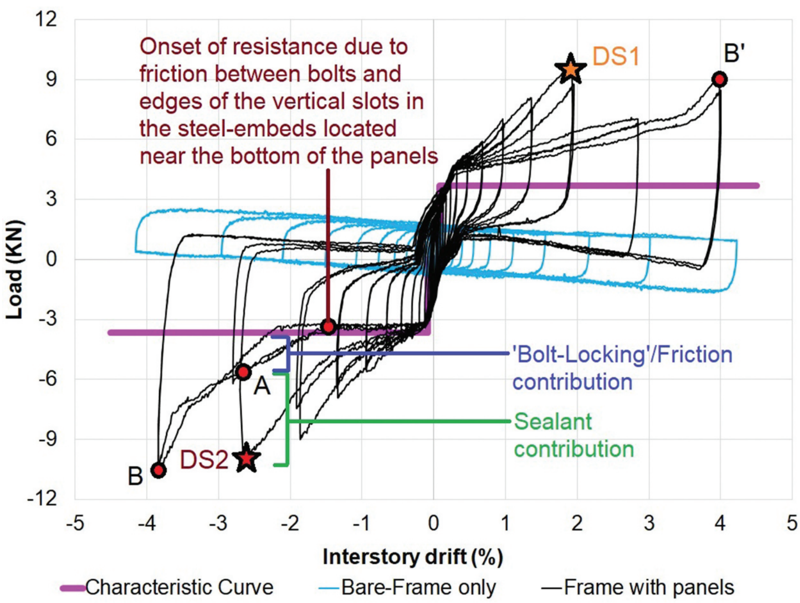

Figure 28. Experimental force-drift hysteresis loops (DS1 and DS2 are the damage states observed in the sealant corresponding to partial tearing and full tearing of the sealant, respectively).

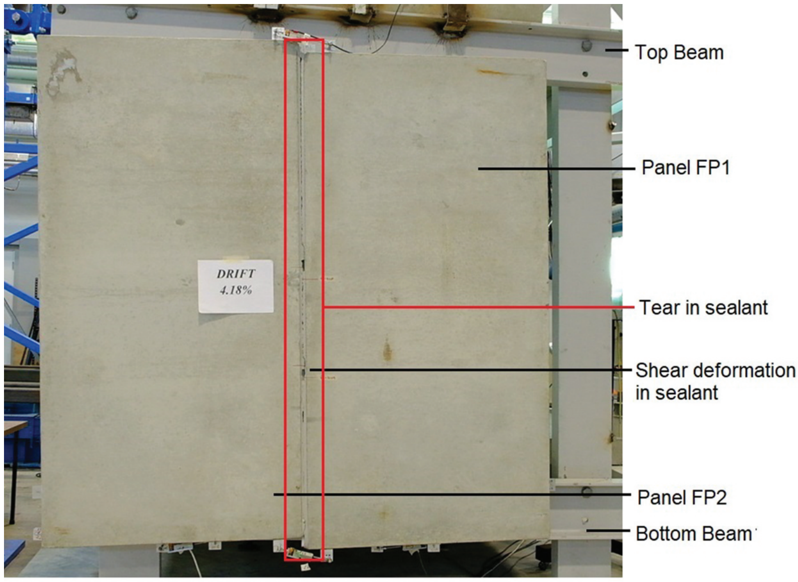

Figure 29. The rocking response of panels and significant tear in the sealant at the peak of the final inter-story drift cycle.

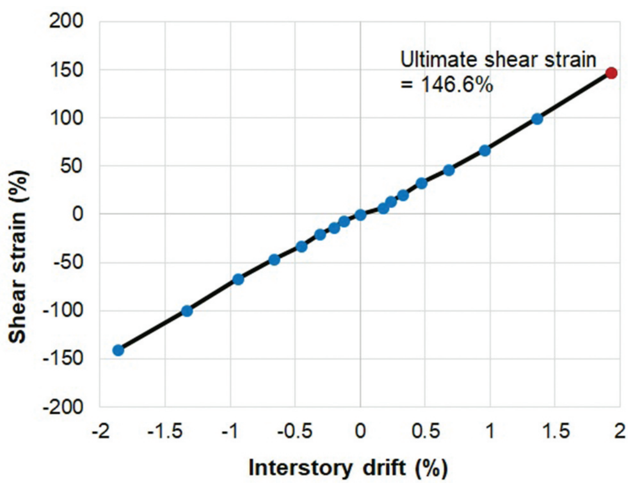

Figure 30. Shear strains in sealant vs. inter-story drift.

Once the panels start rocking, a certain amount of stiffness is provided by shearing resistance in the interposed sealant. The shear strains obtained by dividing the measured shear deformation in the sealant by the width of the sealant corresponding to different inter-story drifts are shown in Fig. 30.

In the hysteretic curve, strength degradation can be observed (within the cycles at the same lateral drift) due to relaxation or tearing of the sealant. The decrease in the lateral force (load) at −2.70% inter-story drift at which the sealant completely tore indicates that the sealant can also significantly contribute to the lateral load resistance during rocking of the panels. Overall, however, the lateral force levels are low as expected.

Even after the complete tearing of the sealant, the panel system is still observed to provide stiffness, resulting in a higher lateral load than that in the characteristic curve. This additional stiffness is attributed to the frictional force developed between the bolts and the sliding edges of the vertical slots, especially at the bottom connections, as the bolts are restrained from moving in the horizontal direction: termed as 'locked' bolts.

To understand the mechanics of the frictional resistance, consider a point 'X_{old}' in the panel, which is located at a horizontal distance of 'l' and vertical distance 't' from the bearing point or rotating point 'O', as shown in Fig. 31.

$$\text{Lever arm}(z) = \sqrt{l^2 + t^2} \tag{29}$$

Initial angle subtended by lever-arm with the horizontal,

$$(\alpha) = \tan^{-1}\left(\frac{t}{l}\right) \tag{30}$$

Now, when the panel rotates by an angle 'θ', the point 'X_{old}' shifts to 'X_{new}' moving a horizontal distance 's'.

$$s = l - z\cos(\alpha + \theta) \tag{31}$$

The lateral drift of 'θ_{lock}' ($s = d_{gap}$), when the bolts lock against the edge of the vertical slot and initiate frictional resistance at the bottom steel-embeds can be calculated as:

$$\Rightarrow \theta_{lock} = \cos^{-1}\left(\frac{l - d_{gap}}{\sqrt{l^2 + t^2}}\right) - \tan^{-1}\left(\frac{t}{l}\right) \tag{32}$$

For panel FP1:

For the bottom-left connections,

$$\theta_{lock(bl-FP1)} = \cos^{-1}\left(\frac{779 - 2}{\sqrt{779^2 + 157^2}}\right) - \tan^{-1}\left(\frac{157}{779}\right) = 0.0124$$

For the bottom-right connections,

$$\theta_{lock(br-FP1)} = \cos^{-1}\left(\frac{11 - 2}{\sqrt{11^2 + 157^2}}\right) - \tan^{-1}\left(\frac{157}{11}\right) = 0.0127$$

For panel FP2:

$$\theta_{lock(bl-FP2)} = \cos^{-1}\left(\frac{764 - 2}{\sqrt{764^2 + 157^2}}\right) - \tan^{-1}\left(\frac{157}{764}\right) = 0.0124$$

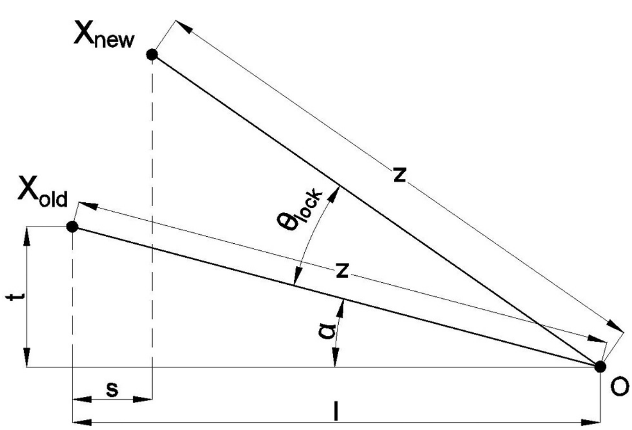

Figure 31. Rotation of a point 'X_{old}' to 'X_{new}' in a panel under rigid body rotation about point 'O'.

$$\theta_{lock(br-FP2)} = \cos^{-1}\left(\frac{11-2}{\sqrt{11^2+157^2}}\right) - \tan^{-1}\left(\frac{157}{11}\right) = 0.0127$$

Therefore, the bolts are expected to 'lock' at an inter-story drift of approximately 1.20%. This value is close to the experimental value, as indicated in Fig. 28. In practice, however, the drift for the onset of 'bolt-locking' may differ from its theoretical value as 'l' and 'd_{gap}' in equation 32 invariably vary, depending upon their exact placements inside the panel and positioning of the panels in a building. It ultimately may lead to some discrepancy in the strengths at a given drift level in the positive and negative direction of the lateral loading (causing asymmetrical force-displacement behavior) . For example, in Fig. 28, the ultimate strength in the negative direction (10.19 kN) is higher than that in the positive direction (9.00 kN). As apparent from the experimental response, the 'bolt-locking' mechanism could potentially help form a secondary load transfer mechanism contributing to the building's response during an extreme earthquake.

The hypothesis on 'bolt-locking' was verified by removing the tack-welds and washers at the bottom connections, allowing the bolts to slide in the horizontal direction effectively (termed as ' horizontally-unrestrained ' bolts), as shown in Fig. 32.

Furthermore, a panel system (without sealant and washers) was subjected to the same loading protocol shown in Fig. 27. The obtained hysteresis loops are plotted in Fig. 33. It can be observed that the characteristic curve can now effectively approximate the backbone of the force-displacement hysteresis of the panel system.

The effect of the 'bolt-locking was quantified by considering the vertical downward force generated at the 'locked' bolt at bottom-left corner steel-embed as 'T' and the corresponding lateral force at the top steel – embeds as 'P_L', as shown in Fig. 34. The horizontal force generated at the 'locked' bolt is ignored as it is near the axis of rotation. Taking moment equilibrium at point 'O' gives,

$$P_L(h_2/\alpha_e) - Tr = 0 \tag{33}$$

$$\Rightarrow P_L = \alpha_e T\left(\frac{r}{h_2}\right) \tag{34}$$

Assuming a critical scenario T = W, where the frictional force in the bolt can withstand the weight of the panel itself, considered to occur at the ultimate limit state 'θ_{ult}':

$$\Rightarrow P_{lock} = \alpha_e W\left(\frac{r}{h_2}\right) \tag{35}$$

where, 'P_{lock}' is the lateral force generated at the top steel-embeds due to 'locking' of bolts in the bottom embeds at the ultimate limit state 'θ_{ult}'.

Figure 32. Bolt connection without tack-welds and washers (termed as 'horizontally-unrestrained' bolts).

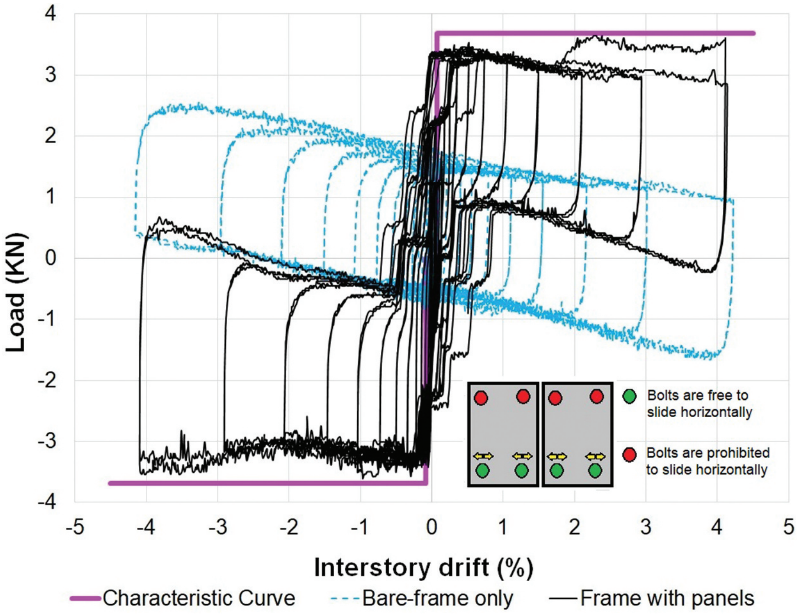

Figure 33. Force-drift hysteresis loops with 'horizontally-unrestrained' bolts at steel-embed connections located near the bottom of the panels (without sealant).

The hysteresis loops of the two adjacent panels, in the absence of the interposed sealant, were obtained and compared, as shown in Fig. 35 with: a)'horizontally-restrained' bolts in one set of diagonal steel-embeds; and b)'horizontally-restrained' bolts in all four steel-embeds. It can be observed that these hysteresis curves are almost the same, which supports the earlier assumption regarding the 'locked-bolt' shown in Fig. 34.

Now, the total lateral force 'P_{total}' generated at the inter-story drift of 'θ_{sc}' when the sealant is expected to tear and at the desired ultimate limit state drift 'θ_{ult}' in the rocking panel system can be calculated by Equations 36 and 37, respectively. These calculated values are shown in Table 1. From Table 1, it can be observed that these equations can closely approximate the maximum loads in the panel system.

$$P_{total}(@\theta_{sc}) = P_{panel} + P_{sealant} + P_{lock}(@\theta_{sc}) \tag{36}$$

$$P_{total}(@\theta_{ult}) = P_{panel} + P_{lock} \tag{37}$$

Where,

'$P_{lock}(@\theta_{sc})$' is the interpolated value of 'P_{lock}' at an inter-story drift of 'θ_{sc}' between 'θ_{lock}' and 'θ_{ult}' assuming a linear interrelationship.

6. The Onset of Damage of the Panel System with Rocking Connections

Visual observations during and after the testing showed no noticeable spalling and cracking of the panels, no yielding of steel, and no loosening of the steel embeds. The damage to the panel system was predominantly localized to the sealant. Damage to the sealant is grouped into the preliminary damage states depending upon their repairability, as defined in Table 2.

According to practitioners, the repairing method depends on the extent and width of the tear in the sealant. If the ratio of the total length of the tear to the total length of sealant in the joint is small, then the sealants can be partially replaced by removing a more significant portion of sealant around the torn

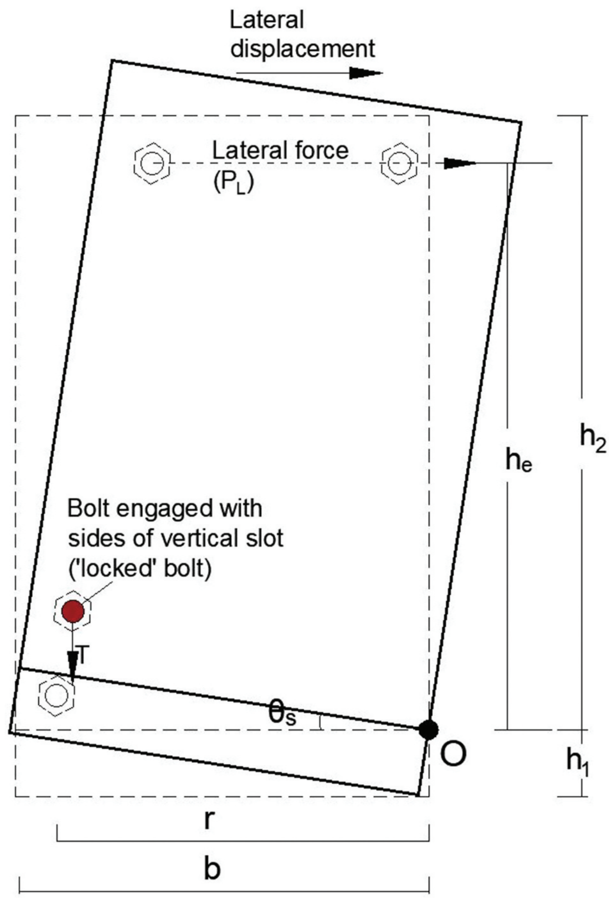

Figure 34. Forces in the panel due to 'locking' of the bolt.

area and reapplying new sealant with similar properties. Sometimes, the tear may not be easily perceived and, therefore, does not significantly affect the aesthetics of the buildings. However, the weather tightness of the joint can be compromised as rainwater can squeeze into the joint due to capillary actions. Such a damaged state is referred to here as Damage State 1 (DS1), and an example is shown in Fig. 36.

On the other hand, if the ratio of the total length of the tear in the sealant to the total length of the sealant in the joint is large (say about 50%; it may vary according to the accessor), then the tear is detected quickly. Such a tear can significantly deteriorate the aesthetics of the building and compromise its weatherproofing functionality. Therefore, the whole sealant must be replaced. Such a damaged state is referred to here as Damage State 2 (DS2), and an example is shown in Fig. 37.

The inter-story drifts corresponding to the damage states DS1 and DS2 of the sealant are 1.92% ($\approx$ 1.84%, estimated from Equation 26) and 2.70%, respectively, as indicated in Fig. 28.

7. Comparison with Conventional Systems

A comparison (Table 3 to Table 7) between the seismic performance of the novel connection and prevalent slotted tie-back and flexible ductile rod is established based on the experiments conducted by several authors. It is acknowledged that this experiment on novel rocking connection details has

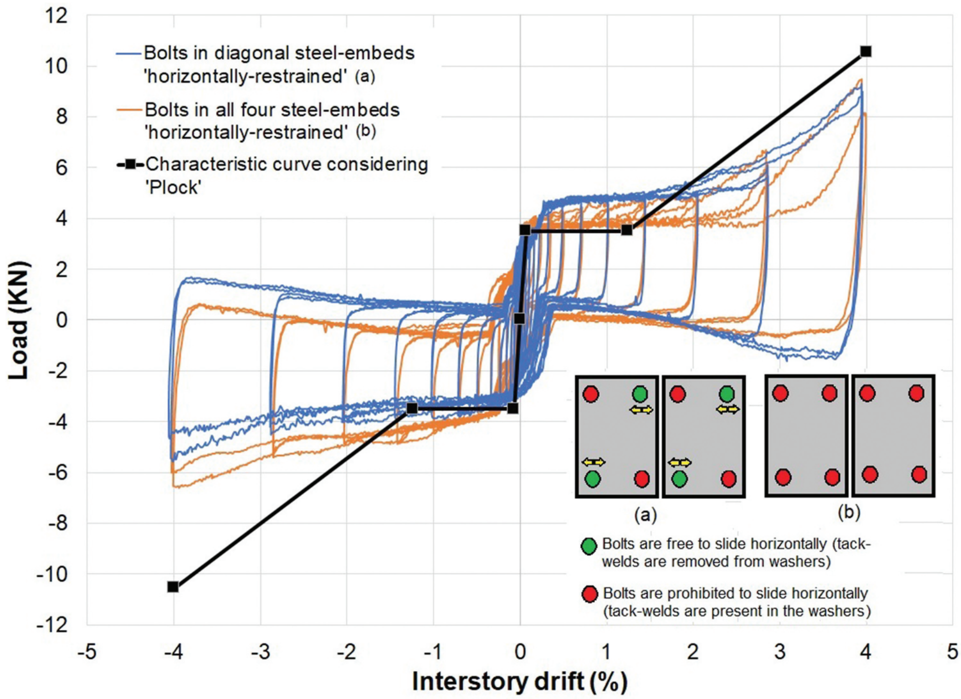

Figure 35. Force-drift hysteresis loops with bolts diagonal steel-embeds 'horizontally-restrained' and with bolts in all four steel-embeds 'horizontally-restrained' (without sealant).

Table 1. Calculated forces vs. Experimental forces.

Calculated force (kN)	From experiment (kN)
$P_{panel} = \frac{1.05(6.1\times1015+6.1\times1015)}{2\times1760} = 3.68$	3.61 (Fig. 33)
$P_{sealant} = \frac{1.05 \times 0.22 \times 1.46(2000 \times 10 \times 1015)}{1760} = 3.61$	=Force at DS2-Force at point A = 9.93–5.64 =4.29 (Fig. 28)
$P_{lock} = \frac{1.05}{1760}(6.1 \times 779 + 6.1 \times 764) = 5.62$	=((Force at Point B-P_{panel})+(Force at Point B′-P_{panel}))/2 =((10.19–3.61)+(9–3.61))/2 = 5.985 (Fig. 28)
$P_{total}(@1.84\%) = \left(\frac{5.62(1.84-1.20)}{4-1.20}\right) + 3.61$	=Force at DS1 =8.98 (Fig. 28)
$P_{total}(@4\%) = 5.62 + 3.68 = 9.3$	=(Load at B+ Load at B′)/2 =(10.19 + 9)/2 = 9.59 (Fig. 28)

Here, $G_s = 0.25\ MPa,\ \gamma_{ult} = 125\%,\ \theta_{sc} = 1.84\%,\ \alpha_e = 1.05,\ and\ \theta_{ult} = 4\%$

Table 2. Preliminary damage states of the sealant.

Damage state	Onset inter-story drift	Method of repair
DS1	1.92%	A larger section to the torn length of sealant (100 mm on each end of the tear) is removed (or scraped off), the surface is cleaned, and new sealant is applied
DS2	2.70%	Entire length of the sealant is removed (or scraped off), the surface is cleaned, and new sealant is applied

several limitations as the effects of dynamic loads, out-of-plane behavior, strain rates on sealant, beam-elongation effects, and types of panels have not been investigated.

Figure 36. Examples of sealant damage corresponding to damage state DS1 after 1.92% inter-story drift.

Figure 37. Examples of sealant damage corresponding to damage state DS2 after −2.70% inter-story drift.

However, this experiment does demonstrate a good performance of the rocking panel system in terms of seismic resiliency. It is not expected that dynamic loads will cause a significant variation in its in-plane performance. Further investigations in the in-plane and out-of-plane performance of the panels in a 3D steel frame are currently being conducted at the University of Canterbury.

Table 3. Seismic performance of horizontal slotted tie-back connections.

Author	Connection Type	Loading	Onset Drift (%)	Damage state
Wang 1987	Short Rod (l/d=0)*#	Cyclic	0.80	Moderate
Baird 2014	Short Rod (l/d=0)#	Cyclic	1.50	None
Pantoli 2016	Short Rod (l/d=0)	Dynamic	1.29	None
Pantoli 2016	Medium Rod (3.5 <l/d<4.7)	Dynamic	0.36	Moderate
Pantoli 2016	Long Rod (7<l/d<9.3)	Dynamic	0.24	Moderate
This study	Steel embeds with vertical slots	Cyclic	3.98	None

**l/d=free length of rod/diameter of rod, # Assumed*

Table 4. Seismic performance of flexing ductile push-pull connections.

Author	Connection Type	Loading	Onset Drift (%)	Damage state
Rihal 1989	Short Rod (l/d=12.5)*	Cyclic	1.20	Severe
Baird 2014	Short Rod (l/d=12.5)	Cyclic	0.50	Moderate
Baird 2014	Short Rod (l/d=12.5)	Cyclic	2.00	Severe
Pantoli 2016	Short Rod (10.9<l/d<14.5)	Dynamic	0.66	None
Pantoli 2016	Medium Rod (14.9<l/d<19.8)	Dynamic	0.66	Moderate
Pantoli 2016	Long Rod (18.9<l/d<25.2)	Dynamic	1.29	Moderate
This study	Steel embeds with vertical slots	Cyclic	3.98	None

**l/d=free length of rod/diameter of rod, # Assumed*

Table 5. Seismic performance of bearing connections.

Author	Connection Type	Loading	Onset Drift (%)	Damage state
Wang 1987	Tube filled with concrete	Cyclic	0.80	Moderate
Wang 1987	Steel Angles	Cyclic	2.50	Severe
This study	Weld-plate and RHS bearing connection	Cyclic	3.98	None

The damage states are defined based on the extent of repairs required (Hutchinson et al. 2014): **None**, when there is no visible damage; **Minor**, if the damage is mostly superficial; **Moderate**, if it requires some repair, and **Severe**, if it is life-threatening.

From Table 3, 4, 5, 6 to Table 7, it is apparent that the cladding panel system incorporating the developed novel rocking connections is seismically more resilient than the panel systems with traditional tie-back or push-pull connections.

Table 6. Seismic performance of panels.

Author	Connection Type	Loading	Onset Drift (%)	Damage state
Pantoli 2016	Slotted/Ductile Threaded Rod	Dynamic	0.24	Minor
Pantoli 2016	Slotted/Ductile Threaded Rod	Dynamic	1.29	Minor
This study	Steel embeds with vertical slots	Cyclic	3.98	None

Table 7. Seismic performance interposed sealant.

Author	Connection Type	Loading	Onset Drift (%)	Damage state
Wang 1987	Short Rod (l/d=0)*#	Cyclic	0.20	Moderate
Pantoli 2016	Slotted/Ductile Threaded Rod	Dynamic	0.66	Minor
Pantoli 2016	Slotted/Ductile Threaded Rod	Dynamic	1.29	Moderate
This study	Steel embeds with vertical slots	Cyclic	1.92	Moderate

**l/d=free length of rod/diameter of rod, # Assumed*

8. Conclusions

A novel rocking connection (comprising steel-embed with vertical slot and weld-plates) is developed for precast concrete cladding panels system in this paper. The slotted steel-embeds are cast-in near the four corners of the panel, which facilitate the rocking motion of the panels under lateral inter-story drifts. They also restrain the panel against in-plane and out-of-plane lateral loads. The two weld-plates are placed near the base of the panels, below the steel-embeds. They avoid any local spalling and chipping of concrete during the rocking of panels.

The steel-embeds and weld plates are designed to satisfactorily resist the horizontal and vertical design actions as per NZS 1170.5, respectively. The length of the vertical slots in the steel embeds is designed to allow the panels to rock up to a specific design inter-story drift and engage in the lateral load resistance mechanism once the slot is exhausted. The design of the vertical inter-panel joint width allows the designer to control even the very first damage state in the panel system (tear in the interposed sealant) depending upon the sealant properties and panel dimensions.

A pair of 2-meter-high adjacent precast concrete cladding panels, incorporating the developed rocking connections, were designed and manufactured. Even though the manufacturing phase of these connections and panels required close supervision, the installation and adjustment of the panels were found to be quick and easy.

The pair of panels were tested under lateral cyclic inter-story drifts following FEMA 461 loading protocol. From the experimental results, it can be concluded that the panels with these rocking connections can accommodate large inter-story drifts ($\approx 4\%$ in this test) without any noticeable damage to the panels and the connections. Even though the theoretical inter-story drift capacity of the panels was around 8%, friction resistance between the edges of the slot in the steel-embed and the bolt shaft occurred much earlier (around 1.20% inter-story drift). The bolts were unable to adequately accommodate the relative horizontal displacements between the panel and the structure during the rocking of the panels, thereby causing a significant rise in the lateral forces. However, this undesired mechanism was avoided simply by removing the tack-welds in the washers, which provided a larger horizontal gap allowing for free horizontal movement of the bolt.

An initial tear in the sealant was noticed at an inter-story drift of 1.92%, close to the anticipated drift of 1.84%. This difference was attributed to the difference in the assumed and actual ultimate shear strain capacities of the sealant.

Comparisons of the seismic performance of the precast concrete cladding panel system incorporating these rocking connections with that of traditional tie-back and push-pull connections from the literature demonstrate its superior seismic resilience.

ORCID

Jitendra Bhatta http://orcid.org/0000-0002-7188-8292
Rajesh P. Dhakal http://orcid.org/0000-0001-5524-5919
Timothy J. Sullivan http://orcid.org/0000-0002-6997-5434

References

ACI 318-11. 2011. Building code requirements for structural concrete and commentary. Farmington Hills, MI: American Concrete Institute Committee.

ACI 533R-93 (American Concrete Institute Committee). 1993. Guide for precast concrete wall panels. USA.

AISC 341-10.2010. Seismic provisions for steel buildings. Chicagi, IL: American Institute of Steel Construction.

ASCE/SEI. 2010. *Minimum design loads for buildings and other structures (ASCE/SEI 7-10)*. Reston, Virginia: American Society of Civil Engineers.

Baird, A. 2014. Seismic performance of precast concrete cladding systems. PhD diss., University of Canterbury.

Baird, A., and H. Ferner. 2017. Damage to non-structural elements in the 2016 Kaikōura earthquake. *Bulletin of the New Zealand Society for Earthquake Engineering* (2): 187–93. doi: 10.5459/bnzsee.50.2.187-193.

Baird, A., A. Palermo, and S. Pampanin. 2011. Facade damage assessment of multi-storey buildings in the 2011 Christchurch earthquake. *Bulletin of the New Zealand Society for Earthquake Engineering*. 44 (4): 368–76. doi:10.5459/bnzsee.44.4.368-376.

Barrett, R. T. 1990. Fastener design manual. 1228. NASA, scientific and technical information division.

Bradley, B. A., R. P. Dhakal, M. Cubrinovski, and G. A. MacRae. 2009. Seismic loss estimation for efficient decision making. *Bulletin of the New Zealand Society of Earthquake Engineering* 42 (2): 96–110. doi: 10.5459/bnzsee.42.2.96-110.

CCANZ. 1992. *Architectural concrete cladding*. New Zealand: Technical Manual.TM-01. Porirua: Cement and Concrete Association of New Zealand.

CERC.2012. Canterbury Earthquakes Royal Commission. Accessed November 10, 2019. https://canterbury.royalcommission.govt.nz/vwluResources/FinalReportVol3Print/$file/Final_Report_Volume_3_Web.pdf

Cohen, J. M. 1995. Literature review on seismic performance of building cladding systems. National Institute of Standards and Technology.

Curtis, M. D. 2014. Physical Characteristics of new houses 2013. Accessed November 20, 2019. https://www.branz.co.nz/

Dal Lago, B., F. Biondini, G. Toniolo, and M. L. Tornaghi. 2017. Experimental investigation on the influence of silicone sealant on the seismic behaviour of precast façades. *Bulletin of Earthquake Engineering*. 15 (4): 1771–87. doi:10.1007/s10518-016-0045-y.

Dal Lago, B. A. 2015. Seismic performance of precast structures with dissipative cladding panel connections. PhD diss., Politecnico Di Milano.

Dhakal, R. P. 2010. Damage to non-structural components and contents in 2010 Darfield earthquake. *Bulletin of the New Zealand Society for Earthquake Engineering* 43 (4): 404–11. doi: 10.5459/bnzsee.43.4.404-411.

Dhakal, R. P., G. MacRae, and K. Hogg. 2011. Performance of ceilings in the February 2011 Christchurch earthquake. *Bulletin of the New Zealand Society of Earthquake Engineering* 44 (4): 377–87. doi: 10.5459/bnzsee.44.4.377-387.

EC8. 2004. *Eurocode 8: Design of structures for earthquake resistance - Part 1: General rules, seismic actions and rules for buildings*. Brussels, Belgium: CEN/TC 250.

English, B.2015. Budget speech. Accessed November 12, 2019. https://treasury.govt.nz/resources/budget-speech-1

FEMA.2007. Interim testing protocols for determining the seismic performance characteristics of structural and non-structural components. FEMA 461. Washington, DC: Federal Emergency Management Agency. Accessed December 19, 2019. https://www.fema.gov/media-library/assets/documents/15207.

FEMA E-74. 2011. *Reducing the risks of nonstructural earthquake damage - A Practical guide*. Washington, DC: Federal Emergency Management Agency.

FEMA P-750. 2009. *NEHRP recommended seismic provisions*. Washinton, DC: Federal Emergency Management Agency.

Folić, R. J. 1991. Classification of damage and its causes as applied to precast concrete buildings. *Materials and Structures* 24 (4): 276–85. doi: 10.1007/BF02472083.

Hunt, J. P. 2010. Seismic performance assessment and probabilistic repair cost analysis of precast concrete cladding systems for multistory buildings. PhD diss., UC Berkely.

Hutchinson, T., E. Pantolli, K. McMullin, M. Hildebrand, and G. Underwood. 2014. Seismic drift compatibility of architectural precast concrete panels and connections: A design guide for engineers. Reporte Técnico No. SSRP-14/16, University of California.

Khakurel, S., R. P. Dhakal, T. Z. Yeow, and S. K. Saha. 2020. Performance group weighting factors for 1 rapid seismic loss estimation of buildings of 2 different usage. *Earthquake Spectra*. doi: 10.1177/8755293019901311.

Khakurel, S., T. Z. Yeow, F. Chen, Z. Wang, S. K. Saha, and R. P. Dhakal. 2019. Development of cladding contribution functions for seismic loss estimation. *Bulletin of the New Zealand Society for Earthquake Engineering* 52 (1): 23–43. doi: 10.5459/bnzsee.52.1.23-43.

Lam, N. T. K., and E. Gad.2002. An innovative approach to the seismic assessment of non-structural components in buildings. *Australian Earthquake Engineering Society (AEES) Annual Seminar.* Adelaide, Australia.

Maness, G. L. 1991. Preventing wall deterioration. *Journal of Property Management* 56 (5): 33–37.

Massey, W. E., L. Megget, and A. Charleson. 2007. *Architectural design for earthquake: A guide to the design of non-structural elements*. New Zealand: Society for Earthquake Engineering.

MBIE. 2004. *Building code B1-structure*. New Zealand: Ministry of Business, Innovation and Employment.

MBIE.2017. Economic benefits of code compliant non-structural elements in new buildings. Ministry of Business, Innovation and Employment. Accessed November 15, 2019. https://www.mbie.govt.nz/assets/decf694d37/economics-relating-to-the-seismic-performance-of-non-structural-elements-v2.pdf

MBIE and EQC. 2017. Secondary Structural and Non-structural Elements-C10. Ministry of Business, Innovation and Employment and Earthquake Commission. Accessed December 18, 2019. www.building.govt.nz

McMullin, K. M., M. Ortiz, L. Patel, S. Yarra, T. Kishimoto, C. Stewart, and B. Steed. 2012. Response of exterior precast concrete cladding panels in NEES-TIPS/NEESGC/E-Defense tests on a full scale 5-story building. *Structures Congress* 2012: 1305–14. doi: 10.1061/9780784412367.117.

Negro, P., and M. L. Tornaghi. 2017. Seismic response of precast structures with vertical cladding panels: The SAFECLADDING experimental campaign. *Engineering Structures* 132: 205–28. doi: 10.1016/j.engstruct.2016.11.020.

NZS 1170.5 - Supp1 (Standards New Zealand).2004. Structural Design Actions, Part 5: Earthquake Actions Commentary.

NZS 1170.5 (Standards New Zealand).2004. Structural design actions, part 5: Earthquake actions.

NZS 3404 (Standards New Zealand).1997. Steel Structures Standard.

Page, I. 2009. Cladding types in New Zealand. *BUILD*: 55-56.

Pantoli, E. 2016. Seismic behavior of architectural precast concrete cladding panels and connections. PhD diss., UC San Diego.

PCI.2007. *Architectural precast concrete*. 3rd ed. Chicago, Illinois: Precast/Prestressed Concrete Institute.

Rihal, S. S. 1989. Earthquake resistance and behavior of APCC and connections. *Architectural Precast Concrete Cladding - Its Contribution to Lateral Resistance of Buildings*, Chicago, IL., USA.

Sack, R. L., R. J. Beers, and D. L. Thomas. 1989. Seismic behavior of architectural precast concrete cladding. *Architectural Precast Concrete Cladding – Its Contribution to Lateral Resistance of Buildings*, Chicago, IL., USA.

SESOC.2019. Interim design guidance: Design of conventional structural systems following the Canterbury Earthquakes 10. Version no.10. New Zealand: Structural Engineering Society New Zealand.

Taghavi, S., and E. Miranda.2003. Response assessment of non-structural building elements. Report 2003/05, University of California Berkeley.

Toniolo, G., and B. Dal Lago. 2017. Conceptual design and full-scale experimentation of cladding panel connection systems of precast buildings. *Earthquake Engineering & Structural Dynamics* 46 (14): 2565–86. doi: 10.1002/eqe.2918.

Villaverde, R. 1997. Seismic design of secondary structures: State of the art. *Journal of Structural Engineering* 123 (8): 1011–19. doi: 10.1061/(ASCE)0733-9445(1997)123:8(1011).

Wang, M. L. 1987. Cladding performance on a full-scale test frame. *Earthquake Spectra* 3.1: 119–73. doi: 10.1193/1.1585423.

Wood, A., I. Noy, and M. Parker. 2016. The Canterbury rebuild five years on from the Christchurch earthquake. *The Reserve Bank of New Zealand Bulletin* 79 (3): 3.